*Organometallics* **1997,** *16,* 4776−4787

# Multistep Redox Processes and Intramolecular Charge Transfer in Ferrocene-Based 2,2′-Bipyridylboronium Salts

Fabrizia Fabrizi de Biani,[†] Thomas Gmeinwieser,[‡] Eberhardt Herdtweck,[‡]
Frieder Jäkle,[‡] Franco Laschi,[†] Matthias Wagner,*,[‡] and Piero Zanello[†]

*Anorganisch-Chemisches Institut der Technischen Universität München, Lichtenbergstrasse 4,*
*D-85747 Garching, Germany, and Universitá di Siena, Dipartimento di Chimica,*
*Pian dei Mantellini 44, 53100 Siena, Italy*

*Received April 22, 1997*[⊗]

A one-step high-yield synthesis of donor−acceptor complexes **[1A]X** to **[1D]X**, **[2A]X**$_2$, and **[4A]X**$_4$ with one, two, and four cationic [B(R)bipy]$^+$ acceptors (R = Me, Br, OEt, NC$_4$H$_8$; X = Br, PF$_6$; bipy = 2,2′-bipyridine) covalently attached to a ferrocene donor is described. Apart from 2,2′-bipyridine, 1,10-phenanthroline and 2,2′-bipyrimidine have also been used as chelating amines. With the exception of R = Br, water-stable compounds are obtained in all cases. In DMF solution and under an inert atmosphere, **[1A]PF**$_6$, **[2A](PF**$_6$**)**$_2$, and **[4A](PF**$_6$**)**$_4$ behave as reversible three-step redox systems, capable of storing three, five, and nine electrons, respectively. In their cationic state, the complexes possess an intense purple color, which can be attributed to charge-transfer interactions between the ferrocene unit and the electron-poor B(R)bipy substituent(s). This is confirmed by the ESR spectrum of the monoreduced species **[1A]**$^0$, which features a line shape indicating considerable admixture of the ligand and metal orbitals.

## Introduction

Coordinating electron-poor ligands or aromatic systems with highly polarizable $\pi$ electrons to an organometallic compound having weakly bound valence electrons may yield electronic structures with interesting applications, for example, in the field of electronic devices,[1−4] redox catalysis,[5] or materials with enhanced optical nonlinearities.[6,7] Ferrocene is a viable electron source in donor−acceptor compounds, since it can be switched reversibly between the Fe(II) and Fe(III) state, and its electron-donor ability may be fine-tuned by choice of appropriate substituents.[8] Furthermore, the minimal structural change resulting from the oxidative conversion of ferrocene to the ferricinium cation is symptomatic of the minor reorganization energy requisite for facile electron transfer.[9] Consequently, detailed information has been gathered on the intermolecular electronic interaction of ferrocene with a variety of acceptor components, ranging from purely organic molecules to late transition metal complexes.[8] There is, however, still a lack of readily available ferrocene-containing donor−acceptor complexes with both units covalently attached to each other.[10,11] These systems deserve particular interest, because their well-defined architecture helps to study even weak interactions and makes it possible to investigate the dependence of electronic charge transfer (CT) on the relative orientation of the donor and acceptor unit.

Our group has developed methods to employ the spontaneous formation of boron−nitrogen(phosphorus) bonds for the facile synthesis of sophisticated target structures like *ansa*-metallocenes[12,13] or oligometallic complexes,[14,15] which would be much harder to make by conventional organic synthesis. An extension of this approach into the field of ferrocene-based donor−acceptor compounds and multiredox systems is presented in this paper. Our aim is (i) to investigate the potential of 2,2′-bipyridylboronium salts **[I]**$^+$ (Figure 1) as novel electron acceptors in ferrocene-containing CT complexes and (ii) to demonstrate a facile route to ferrocenes covalently connected with these acceptors.

Cations **[I]**$^+$ are relatives of the well-known diquat, **[II]**$^{2+}$, which possesses an ethylene bridge instead of the BRR′ unit and behaves as a perfectly reversible two-step redox system.[16] A similar electrochemical behavior is found in the case of **[I]**$^+$ (Figure 1), where, moreover,

---

[†] Universitá di Siena. Telefax: +39-577-280405. E-mail: zanello@unisi.it.

[‡] Technische Universität München. Telefax: +49-89-28913473. E-mail: wagner@arthur.anorg.chemie.tu-muenchen.de.

[⊗] Abstract published in *Advance ACS Abstracts,* September 15, 1997.

(1) Hale, P. D.; Inagaki, T.; Karan, H. I.; Okamoto, Y.; Skotheim, T. A. *J. Am. Chem. Soc.* **1989**, *111*, 3482.

(2) Astruc, D. *New J. Chem.* **1992**, *16*, 305.

(3) Bard, A. J. *Nature* **1995**, *374*, 13.

(4) Alonso, B.; Morán, M.; Casado, C. M.; Lobete, F.; Losada, J.; Cuadrado, I. *Chem. Mater.* **1995**, *7*, 1440.

(5) Astruc, D. *Angew. Chem.* **1988**, *100*, 662; *Angew. Chem., Int. Ed. Engl.* **1988**, *27*, 643.

(6) Calabrese, J. C.; Cheng, L.-T.; Green, J. C.; Marder, S. R.; Tam, W. *J. Am. Chem. Soc.* **1991**, *113*, 7227.

(7) Kanis, D. R.; Ratner, M. A.; Marks, T. J. *J. Am. Chem. Soc.* **1992**, *114*, 10338.

(8) *Ferrocenes*; Togni, A., Hayashi, T., Eds.; VCH Verlagsgesellschaft: Weinheim, Germany, 1995.

(9) Yang, E. S.; Chan, M.-S.; Wahl, A. C. *J. Phys. Chem.* **1980**, *84*, 3094.

(10) Green, M. L. H.; Marder, S. R.; Thompson, M. E.; Bandy, J. A.; Bloor, D.; Kolinsky, P. V.; Jones, R. J. *Nature* **1987**, *330*, 360.

(11) Wright, M. E.; Cochran, B. B. *Organometallics* **1993**, *12*, 3873.

(12) Jäkle, F.; Mattner, M.; Priermeier, T.; Wagner, M. *J. Organomet. Chem.* **1995**, *502*, 123.

(13) Herdtweck, E.; Jäkle, F.; Opromolla, G.; Spiegler, M.; Wagner, M.; Zanello, P. *Organometallics* **1996**, *15*, 5524.

(14) Jäkle, F.; Priermeier, T.; Wagner, M. *Chem. Ber.* **1995**, *128*, 1163.

(15) Fabrizi de Biani, F.; Jäkle, F.; Spiegler, M.; Wagner, M.; Zanello, P. *Inorg. Chem.* **1997**, *36*, 2103−2111.

(16) Hünig, S.; Wehner, I. *Heterocycles* **1989**, *28*, 359.

S0276-7333(97)00345-2 CCC: $14.00

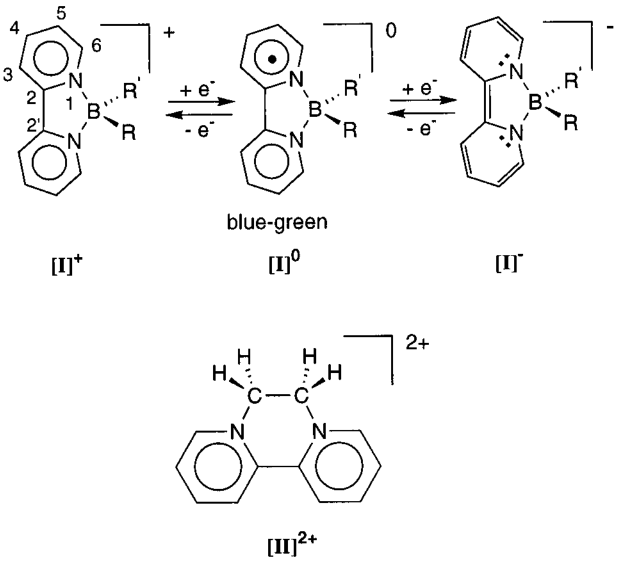

**Figure 1.** Two-step reduction of 2,2′-bipyridylboronium cations **[I]**$^+$ and their carbon−nitrogen analogue diquat **[II]**$^{2+}$.

considerable changes of its redox potential on varying the boron substituents R and R′ have been observed.[16]

## Results and Discussion

**Selection of Compounds.** We will specify the nature of the counteranion(s) $X^-$ ($X^- = Br^-$, $PF_6^-$) only in those cases where different structural features or a different chemical behavior may be anticipated. Compounds **[1A]X**, **[2A]X$_2$**, and **[4A]X$_4$**, bearing one, two, and four acceptor units, respectively, have been synthesized to study the influence of an increasing number of cationic substituents on the Fe(II)/Fe(III) redox potential of the central iron atom (Scheme 1). Moreover, we are interested in the degree of electronic communication between different 2,2′-bipyridylboronium moieties attached to the same ferrocene backbone. Compounds with three boron substituents have not been investigated due to the lack of selective routes to the starting material 1,1′,3-Fe[$C_5H_3(BBr_2)_2$][$C_5H_4(BBr_2)$] **3**.[17]

Compared to 2,2′-bipyridine (bipy), 1,10-phenanthroline (phen) possesses a more rigid framework, together with an extended $\pi$ system. The phenanthroline derivative **[1E]X** (Figure 2) makes it possible to investigate the impact of these parameters on the stability of the boronium cations on one hand and their electrochemical behavior on the other. We have also included the 2,2′-bipyrimidine (bipm) derivative **[1F]Br** (Figure 2) in our study since its two unoccupied nitrogen donors may still act as ligands to transition metals. This provides a way of tuning the acceptor quality of the aromatic heterocycle by choice of selected coordinating complex fragments.

To investigate the consequences of cutting the carbon−carbon bridge connecting both pyridine rings on the stability of the ferrocenylboronium cation, as well as on its electron-accepting properties, we have prepared the $\gamma$-picoline derivative **[1G]Br** (Figure 2).

**Scheme 1. Synthesis of 2,2′-Bipyridyl(ferrocenyl)boronium Salts**[a]

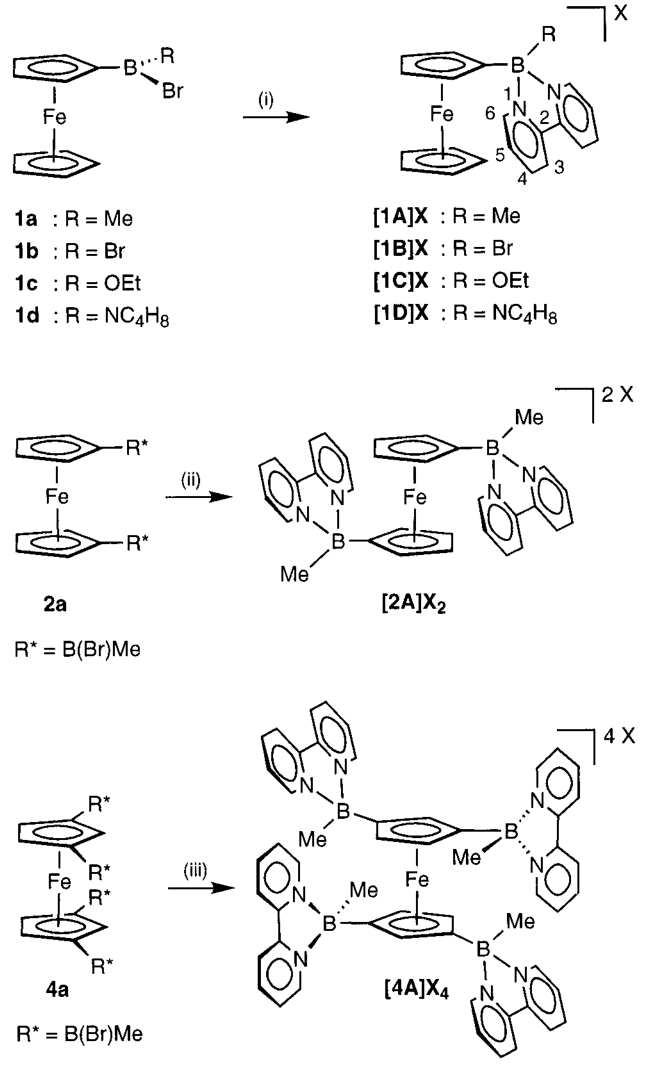

[a] Key: (i) **[1A,C,D]PF$_6$**: +1bipy (toluene, −60 °C) + excess $NH_4PF_6$ (water, ambient temperature). **[1B]Br**: +1bipy ($CH_2Cl_2$, −78 °C). (ii) +2bipy ($CH_2Cl_2$, −60 °C) + excess $NH_4PF_6$ (water, ambient temperature). (iii) +4bipy ($CH_2Cl_2$, −60 °C) + excess $NH_4PF_6$ (water, ambient temperature). $X = Br^-$, $PF_6^-$.

**Syntheses and NMR Spectroscopy.** The Br salts **[1A−D]Br**, **[2A]Br$_2$**, and **[4A]Br$_4$** are obtained in very high yield by the reaction of ferrocenylboranes **1a-d**,[18,19] **2a**,[20] and **4a**[21] with 2,2′-bipyridine in either toluene or $CH_2Cl_2$ solution (Scheme 1).

**[1E]Br** was synthesized from **1a** and 1 equiv of 1,10-phenanthroline in the same way as its bipy analogue **[1A]Br**. **[1F]Br** is available in high yield by simply mixing **1a** with 1 equiv of 2,2′-bipyrimidine; dimetallic complexes [FcB(Me)−bipm−B(Me)Fc]$^{2+}$ were not observed. An initially apparent peculiarity of all the ferrocene-based boronium cations described so far is their intense purple color both in the solid state and in solution (see below). In contrast, **[1G]Br** is a pale yellow microcrystalline solid, which was obtained by dissolving **1a** in dry $\gamma$-picoline.

---

(17) Wrackmeyer, B.; Dörfler, U.; Herberhold, M. *Z. Naturforsch.* **1993**, *48b*, 121.

(18) Renk, T.; Ruf, W.; Siebert, W. *J. Organomet. Chem.* **1976**, *120*, 1.

(19) Jäkle, F.; Priermeier, T.; Wagner, M. *Organometallics* **1996**, *15*, 2033.

(20) Ruf, W.; Renk, T.; Siebert, W. *Z. Naturforsch.* **1976**, *31b*, 1028.

(21) Appel, A.; Nöth, H.; Schmidt, M. *Chem. Ber.* **1995**, *128*, 621.

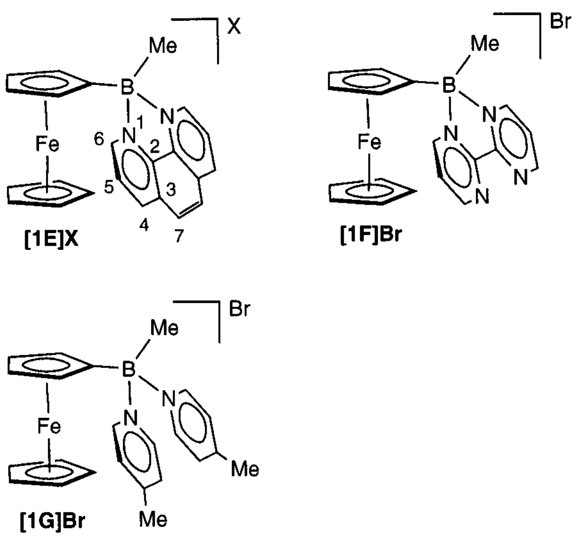

**Figure 2.** The ferrocene-based boronium cations **[1E]X** and **[1F,G]Br**.

**Scheme 2. Nucleophilic Substitution of $Br^-$ in $[\mathbf{1B}]^{+a}$**

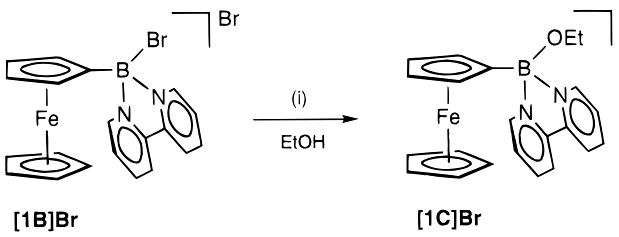

[a] Key: (i) + $NEt_3$.

Except for $[\mathbf{1B}]^+$, all of the 2,2′-bipyridyl(ferrocenyl)boronium cations are inert toward air and moisture. In the case of $[\mathbf{1B}]^+$, however, the Br substituent at boron is readily replaced by water and other nucleophiles. This has been proven, for example, by treating the compound with EtOH in the presence of $NEt_3$, which gives **[1C]Br** in quantitative yield (Scheme 2). The nucleophilic substitution of bromide in $[\mathbf{1B}]^+$ may, thus, serve as a useful synthetic route to derivatives bearing substituents R, which are not compatible with the highly Lewis acidic boron centers in the starting materials FcB(R)Br (Fc = $(C_5H_5)Fe(C_5H_4)$).

The $PF_6$ salts $\mathbf{[1A]PF_6}$, $\mathbf{[1C\text{-}E]PF_6}$, $\mathbf{[2A](PF_6)_2}$, and $\mathbf{[4A](PF_6)_4}$ can be precipitated quantitatively from aqueous solutions of the corresponding Br salts upon treatment with $NH_4PF_6$. Due to their pronounced sensitivity toward air and moisture, **[1B]Br** and **[1G]Br** were not transformed into the corresponding $PF_6$ salts.

The NMR spectra of compounds **[1A–G]X** in $CD_3CN$ solution all exhibit the same general features, which will, thus, be discussed in more detail only for $\mathbf{[1A]PF_6}$. In the $^{11}B$ NMR spectrum of this compound, a resonance at $\delta(^{11}B) = 8.6$ indicates the presence of tetracoordinated boron nuclei. The $^1H$ and $^{13}C$ NMR spectra show only one set of signals for the ferrocene fragment, as well as for the bipy ligand. This finding is most likely explained by the assumption of an unhindered rotation around the B–C axis. Assignments of the $^1H$ and $^{13}C$ NMR resonances of $\mathbf{[1A]PF_6}$ are based on $^1H/^1H$ COSY spectra and 2D heteronuclear shift correlations. The chemical shifts of all other monocations $[\mathbf{1B{-}E}]^+$ were assigned according to these results; the numbering schemes are given in Scheme 1 and Figure 2. The $^1H$ and $^{13}C$ NMR resonances of the ferrocene fragment of $\mathbf{[1A]PF_6}$ lie in the usually observed ranges. All proton signals of the coordinating bipy ligand appear at lower field compared to the free base. In contrast, an upfield shift of 10.9 and 6.0 ppm is observed upon coordination for C-2,2′ ($\mathbf{[1A]PF_6}$, 146.0 ppm; bipy, 156.9 ppm[22] ) and C-6,6′ ($\mathbf{[1A]PF_6}$, 144.1 ppm; bipy, 150.1 ppm), respectively. The other carbon atoms are deshielded by 2.2 (C-3,3′; $\mathbf{[1A]PF_6}$, 123.7 ppm; bipy, 121.5 ppm), 7.3 (C-4,4′; $\mathbf{[1A]PF_6}$, 145.2 ppm; bipy, 137.9 ppm), and 4.6 ppm (C-5,5′; $\mathbf{[1A]PF_6}$, 129.4 ppm; bipy, 124.8 ppm). Analogous, however more pronounced, changes are reported for the $^1H$ and $^{13}C$ NMR spectrum of diquat $[\mathbf{II}]^{2+}$ (Figure 1).[22,23] The NMR resonances of the B(Me)bipy fragments in the diborylated compound $\mathbf{[2A](PF_6)_2}$ are virtually identical with those of $\mathbf{[1A]PF_6}$. It has to be concluded, therefore, that the two cationic moieties attached to the same ferrocene core have no mutual influence on their magnetic environments. Again, there is no indication for rotational hindrance at ambient temperature in $\mathbf{[2A](PF_6)_2}$. This situation changes when two more B(Me)bipy substituents are grouped around the ferrocene backbone. At 20 °C, a solution of $\mathbf{[4A](PF_6)_4}$ in DMSO-$d_6$ shows two resonances for the four methyl groups in the $^1H$ NMR spectrum ($\delta(^1H) =$ 0.27, 0.70). The six ferrocene protons give rise to three signals at 2.53, 3.24, and 4.87 ppm. When the sample is heated, coalescence of both the methyl resonances ($T_c$ = 400 ± 5 K; $\Delta\nu = 170$ Hz) and the signals at 2.53 and 3.24 ppm is observed. From these data, the barrier to rotation around the B–C bond may be estimated to be $\Delta G^\ddagger = 79 \pm 2$ kJ/mol ($\Delta G^\ddagger = 19.14T_c\,(10.32 + \log(T_c\,k_c^{-1}))$; $k_c = 2.22\Delta\nu$[24] ). At ambient temperature, the proton resonances of the bipy ligand appear as eight virtual triplets and eight doublets. Even at 170 °C the signal pattern in the aromatic region of the spectrum is still much more complicated than in the case of $\mathbf{[2A](PF_6)_2}$. Similar features as discussed for the proton spectrum are found in the $^{13}C$ NMR spectrum. These cited observations clearly are the result of a pronouncedly hindered rotation around the B–C bonds in the sterically congested tetracation. The NMR spectra can easily be interpreted if we assume $[\mathbf{4A}]^{4+}$ to possess a $C_2$ axis as the only element of symmetry in solution. The same conformation is found in the solid state (see below).

**Molecular Structures of $\mathbf{[1A]PF_6}$, $\mathbf{[2A](PF_6)_2}$, and $\mathbf{[4A]Br_4}$ in the Solid State.** Deep purple X-ray quality crystals of $\mathbf{[1A]PF_6}$ (monoclinic; space group $P2_1$) and $\mathbf{[2A](PF_6)_2}$ (monoclinic; space group $P2_1/c$) were grown by layering their acetonitrile solutions with diethyl ether. Black $\mathbf{[4A]Br_4}$ crystallizes from ethanol (96%) upon slow evaporation of the solvent in the monoclinic space group $C2/c$ (Tables 1 and 2; Figures 3–5). The complete set of structure data for $\mathbf{[1A]PF_6}$, $\mathbf{[2A](PF_6)_2}$, and $\mathbf{[4A]Br_4}$ is available on request.[25]

In all cases, the Bbipy units exhibit a planar conformation with torsion angles between both pyridyl rings

---

[22] Rieger, A. L.; Rieger, P. H. *J. Phys. Chem.* **1984**, *88*, 5845.

[23] Kalinowski, H.-O.; Berger, S.; Braun, S. *$^{13}$C-NMR-Spektroskopie*; Thieme Verlag: Stuttgart, Germany, 1984.

[24] Friebolin, H. *Basic One and Two Dimensional NMR Spectroscopy*; Verlag Chemie: Weinheim, Basel, Cambridge, New York, 1992.

**Table 1. Summary of Crystallographic Data for [1A]$PF_6$, [2A]$(PF_6)_2$, and [4A]$Br_4$**

| | **[1A]$PF_6$** | **[2A]$(PF_6)_2$** | **[4A]$Br_4$** |
|---|---|---|---|
| formula | $C_{21}H_{20}BF_6FeN_2P$ | $C_{32}H_{30}B_2F_{12}FeN_4P_2$ | $C_{54}H_{50}B_4Br_4FeN_8{\cdot}7.75H_2O$ |
| fw | 512.02 | 838.02 | 1369.37 |
| cryst dimens, mm | 0.86 × 0.61 × 0.20 | 0.43 × 0.41 × 0.33 | 0.43 × 0.26 × 0.26 |
| cryst syst | monoclinic | monoclinic | monoclinic |
| space group | $P2_1$ (No. 4) | $P2_1/c$ (No. 14) | $C2/c$ (No.15) |
| temp, K | 193 | 163 | 193 |
| $a$, Å | 7.3075(5) | 9.1984(7) | 11.7038(7) |
| $b$, Å | 11.3931(7) | 14.8407(6) | 23.4915(10) |
| $c$, Å | 13.0388(11) | 12.193(1) | 22.6688(17) |
| $\alpha$, deg | 90 | 90 | 90 |
| $\beta$, deg | 97.755(7) | 100.851(4) | 104.157(7) |
| $\gamma$, deg | 90 | 90 | 90 |
| $V$, $Å^3$ | 1075.6(1) | 1634.7(2) | 6043.3(7) |
| $D_{calcd}$, g $cm^{-3}$ | 1.581 | 1.703 | 1.505 |
| $Z$ | 2 | 2 | 4 |
| radiation | Mo K$\alpha$, 0.710 73 Å | Cu K$\alpha$, 1.541 84 Å | Mo K$\alpha$, 0.710 73 Å |
| no. of total reflns | 8063 | 6242 | 23 364 |
| no. of unique reflns | 3971 | 2913 | 5651 |
| no. of obsd reflns | 3971 (all data) | 2913 ($I > 0$) | 5651 (all data) |
| no. of params | 288 | 302 | 360 |
| $\mu$, $cm^{-1}$ | 8.4 | 55.6 | 29.5 |
| final R1[a] | 0.0448 | 0.0325 | 0.0587 |
| final wR2[b] | 0.1065 | 0.0806 | 0.0840 |
| GOOF[c] | 1.056 | 1.067 | 0.923 |

[a] $R1 = \Sigma(||F_o| - |F_c||)/\Sigma|F_o|$. [b] $wR2 = [\Sigma w\,(F_o^2 - F_c^2)^2/\Sigma w\,(F_o^2)^2\,]^{1/2}$. [c] $GOOF = [\Sigma w(F_o^2 - F_c^2)^2/(NO - NV)]^{1/2}$.

**Table 2. Selected Bond Lengths (Å), Angles (deg), and Dihedral Angles (deg) of [1A]$PF_6$, [2A]$(PF_6)_2$, and [4A]$Br_4$**

| | **[1A]$PF_6$** | **[2A]$(PF_6)_2$** | **[4A]$Br_4$** |
|---|---|---|---|
| B(1) −C(1)[a] | 1.599(4) | 1.589(4) | 1.586(6) [1.598(6)][b] |
| B(1) −C(11) | 1.592(4) | 1.596(3) | 1.594(6) [1.585(5)] |
| B(1) −N(21) | 1.613(4) | 1.589(3) | 1.602(5) [1.603(5)] |
| B(1) −N(31) | 1.580(4) | 1.597(3) | 1.595(4) [1.597(5)] |
| N(21) −C(26) | 1.360(4) | 1.356(3) | 1.354(4) [1.352(4)] |
| N(31) −C(36) | 1.352(4) | 1.354(3) | 1.354(4) [1.352(5)] |
| C(26) −C(36) | 1.457(5) | 1.466(3) | 1.466(5) [1.455(6)] |
| N(21) −B(1) −N(31) | 94.9(2) | 95.2(2) | 94.7(3) [94.8(3)] |
| N(21) −B(1) −C(1) | 109.7(3) | 112.3(2) | 110.7(3) [109.4(3)] |
| N(31) −B(1) −C(1) | 114.0(2) | 111.7(2) | 109.9(3) [110.2(3)] |
| N(21) −B(1) −C(11) | 108.8(2) | 110.7(2) | 105.2(3) [108.2(3)] |
| N(31) −B(1) −C(11) | 108.8(2) | 112.1(2) | 114.4(3) [112.4(3)] |
| C(1) −B(1) −C(11) | 118.1(2) | 113.6(2) | 119.1(3) [119.0(3)] |
| B(1) −N(21) −C(26) | 112.5(2) | 113.3(2) | 113.5(3) [113.1(3)] |
| B(1) −N(31) −C(36) | 113.8(2) | 113.0(2) | 113.6(3) [113.1(3)] |
| N(21) −C(26) −C(36) | 109.2(3) | 109.0(2) | 109.0(3) [109.3(3)] |
| N(31) −C(36) −C(26) | 109.4(3) | 109.2(2) | 109.2(3) [109.6(3)] |
| C(25) −C(26) −C(36) | 129.7(3) | 129.1(2) | 129.4(3) [129.4(3)] |
| C(35) −C(36) −C(26) | 128.5(3) | 128.9(2) | 129.5(3) [129.2(4)] |
| C(25) −C(26) −C(36) −C(35) | −2.2(5) | −0.3(4) | 0.6(6) [−2.0(7)] |
| C(1) −B(1) −C(11) −C(12) | 39.7(4) | −66.2(3) | 34.8(5) [−38.9(5)] |

[a] In the case of **[1A]$PF_6$** and **[2A]$(PF_6)_2$**, B(1) is normally abbreviated as B. [b] Numbers in brackets refer to the corresponding bond lengths and angles in the second B(Me)bipy substituent.

ranging from 0.3(4)° to 2.2(5)° (absolute values). The heterocyclic ring system in **[1A]$PF_6$** shows two significantly different boron−nitrogen bond lengths (B−N(21), 1.613(4) Å; B−N(31), 1.580(4) Å), while all B−N bonds in the higher substituted derivatives **[2A]$(PF_6)_2$** and **[4A]$Br_4$** are equal within experimental error. The distorted geometry of the $BN_2C_2$ five-membered ring in **[1A]$PF_6$** is, thus, most likely the result of crystal packing forces. A comparison of the cationic substituents with the analogous uncharged **1H**[26] and **1I**[27] complexes is particularly revealing (Figure 6).

The latter compounds, which are closely related to the B(Me)bipy substituents under investigation here, offer the opportunity to compare prototype covalent (B−N*) and dative (B−N) boron−nitrogen bonds in the same molecule. As expected, the dative B−N bonds are longer (**1H**, 1.629(7) Å; **1I**, 1.584(17) Å) than their covalent counterparts (**1H**, 1.500(6) Å; **1I**, 1.490(17) Å). The differences between both binding modes appear to be more pronounced in **1H** ($\Delta_{B-N}$ = 0.129 Å) than in **1I** ($\Delta_{B-N}$ = 0.094 Å), which has been attributed to the lower Lewis acidity of the $BF_2$ group compared to the $BBr_2$ fragment. The coordinative B−N bonds to the formally positively charged boron centers of **[1A]**$^+$, **[2A]**$^{2+}$, and **[4A]**$^{4+}$ possess the same lengths as the related B−N

---

(25) Further details of the crystal structure investigations are available on request from the Fachinformationszentrum Karlsruhe, Gesellschaft für wissenschaftlich-technische Information mbH, D-76344 Eggenstein-Leopoldshafen, Germany, on quoting the depository numbers CSD 407665 ([**1A**]**$PF_6$**), CSD 407666 ([**2A**]**$(PF_6)_2$**), CSD 407664 ([**4A**]**$Br_4$**), the names of the authors, and the literature citation.

(26) Klebe, G.; Hensen, K.; Fuess, H. *Chem. Ber.* **1983**, *116*, 3125.

(27) Klebe, G.; Tranqui, D. *Inorg. Chim. Acta* **1984**, *81*, 1.

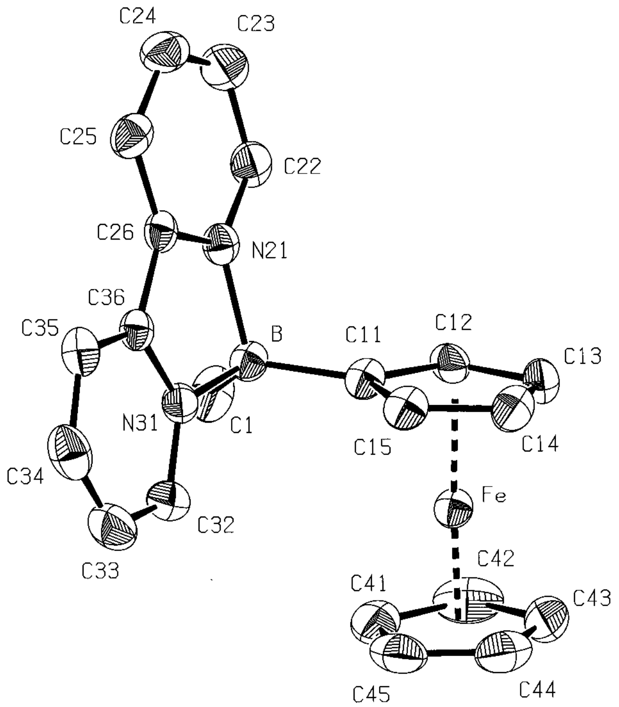

**Figure 3.** PLATON plot of **[1A]PF$_6$** (hydrogen atoms and PF$_6^-$ counterions omitted for clarity; thermal ellipsoids at the 50% probability level).

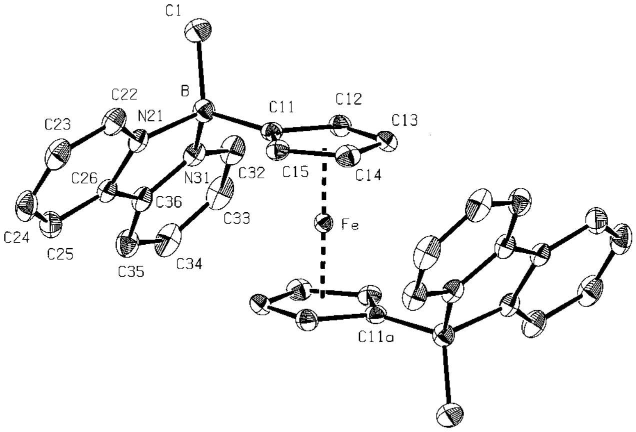

**Figure 4.** PLATON plot of **[2A](PF$_6$)$_2$** (hydrogen atoms and PF$_6^-$ counterions omitted for clarity; thermal ellipsoids at the 50% probability level).

bonds in **1H** and **1I**. This is a noticeable feature since donor−acceptor interactions involving positively charged acceptor atoms tend to be significantly stronger than dative bonds to the respective neutral centers.[28,29] Shorter B−N bonds in 2,2′-bipyridylboronium cations are obviously not prevented by the rigid geometry of the bipy ligand, considering that the analogous C−C bond lengths in the isoelectronic all-carbon framework of fluorene have much smaller values of 1.504(2) Å.[30] The comparatively long B−N bonds in **[1A]$^+$**, **[2A]$^{2+}$**, and **[4A]$^{4+}$**, thus, indicate that the positive charge of the B(Me)bipy group is not located at the boron center but spread over the whole aromatic ring system. This view is supported by a population analysis based on MNDO calculations on the model system [Me$_2$Bbipy]$^+$ (see below).

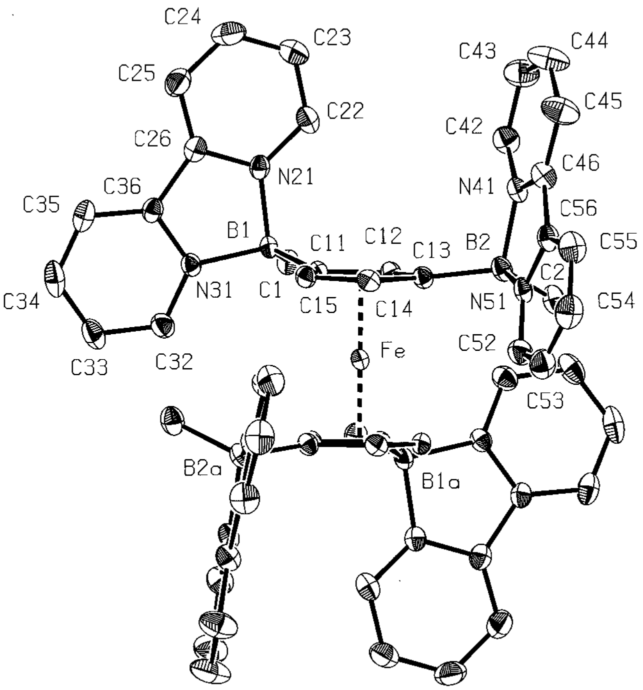

**Figure 5.** PLATON plot of **[4A]Br$_4$** (hydrogen atoms, Br$^-$ counterions, and water molecules omitted for clarity; thermal ellipsoids at the 50% probability level).

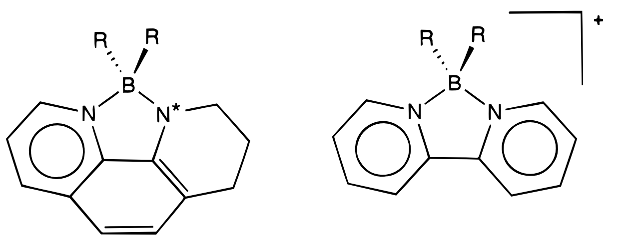

**1H** : R = F
**1I** : R = Br

**[1J]$^+$** : R = C$_6$H$_5$
**[1K]$^+$** : R = Me

**Figure 6.** The iron-free reference systems **1H**, **1I** and **[1J]$^+$**, **[1K]$^+$**.

The coordination of the small boron centers results in a slight distortion of the chelating 2,2′-bipyridine ligands. In the case of **[1A]PF$_6$**, for example, the angles C(25)−C(26)−C(36) and C(35)−C(36)−C(26) on the outer frame of the aromatic system are stretched to values of 129.7(3)° and 128.5(3)°, respectively. Consequently, the angles N(21)−C(26)−C(36) and N(31)−C(36)−C(26) on the inside of the five-membered heterocycle are compressed to values of 109.2(3)° and 109.4(3)°.

The position of the B(Me)bipy substituents in **[2A](PF$_6$)$_2$** leads to a boxlike arrangement of aromatic rings embedding the central iron atom (torsion angle C(1)−B−C(11)−C(12) = −66.2(3)°) and results in short Fe−bipy through-space distances (Fe···COG = 3.74 Å; COG = center of gravity of the BN(21)C(26)C(36)N(31) ring). Different conformations than in the case of **[2A](PF$_6$)$_2$** are found for **[1A]PF$_6$** (torsion angle C(1)−B−C(11)−C(12) = 39.7(4)°) and **[4A]Br$_4$** (C(1)−B(1)−C(11)−C(12) = 34.8(5)°; C(2)−B(2)−C(13)−C(12) = −38.9(5)°). Nevertheless, similarly close distances between iron and the acceptor system are found in all three molecules, and

---

[28] Haaland, A. *Angew. Chem.* **1989**, *101*, 1017; *Angew. Chem., Int. Ed. Engl.* **1989**, *28*, 992.

[29] Jonas, V.; Frenking, G.; Reetz, M. T. *J. Am. Chem. Soc.* **1994**, *116*, 8741.

[30] Gerkin, R. E.; Lundstedt, A. P.; Reppart, W. J. *Acta Crystallogr.* **1984**, *C40*, 1892.

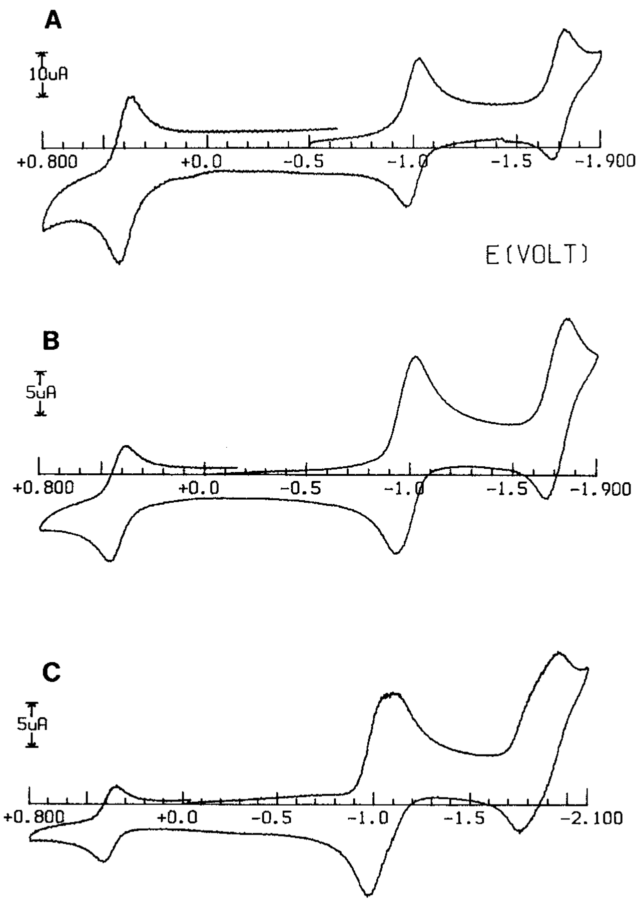

**Figure 7.** Cyclic voltammograms recorded at a platinum electrode on DMF solutions containing [NEt$_4$][PF$_6$] (0.2 mol dm$^{-3}$) and (a) **[1A]PF$_6$** (0.8 × 10$^{-3}$ mol dm$^{-3}$), (b) **[2A](PF$_6$)$_2$** (0.6 × 10$^{-3}$ mol dm$^{-3}$), (c) **[4A](PF$_6$)$_4$** (0.5 × 10$^{-3}$ mol dm$^{-3}$). Scan rate = 0.2 V s$^{-1}$.

the exact position of the B(Me)bipy fragment relative to the ferrocene core seems to be governed mainly by steric interactions and crystal packing effects. It is worth mentioning that most 9-arylfluorenes feature a relative orientation between the aryl ring and the pendant fluorenyl substituent which is very much the same as the one found between the Cp rings and the B(Me)bipy moieties in **[1A]PF$_6$** and **[4A]Br$_4$**.[31,32]

**Electrochemistry.** Figure 7, which shows the cyclic voltammetric behavior of **[1A]PF$_6$**, **[2A](PF$_6$)$_2$**, and **[4A](PF$_6$)$_4$** in DMF solution, gives an overall picture of the high redox aptitude of their 2,2′-bipyridyl(ferrocenyl)boronium cations.

All complexes display one chemically reversible oxidation and two consecutive reversible reduction processes. The relative peak-heights of the cathodic and anodic steps in **[1A]PF$_6$**, **[2A](PF$_6$)$_2$**, and **[4A](PF$_6$)$_4$** reflect the ratio between the number of 2,2′-bipyridylboronium substituents and the ferrocene backbone. Controlled potential coulometric tests of **[1A]PF$_6$**, **[2A](PF$_6$)$_2$**, and **[4A](PF$_6$)$_4$** show that (a) oxidation ($E_w = +0.6$ V) in all cases consumes one electron per molecule. As a consequence of this electron removal, the original red-violet solutions assume the typical blue color of ferricinium derivatives ($\lambda_{max}$ = 626, 637, and 660 nm, respectively). (b) The first reduction step ($E_w = -1.3$ V) basically consumes one, two, and four electrons per molecule **[1A]PF$_6$**, **[2A](PF$_6$)$_2$**, and **[4A](PF$_6$)$_4$**. Some residual currents slightly higher than the background current persist after such stoichiometric consumptions of electrons, possibly because in the long times of macroelectrolysis, slow decomposition of the instantaneously electrogenerated congeners makes the B(Me)bipy ligand to be released (see below). In summary, it is conceivable that the oxidation process is centered on the ferrocene unit, whereas the reduction processes are centered on the peripheral B(Me)bipy groups.

As a typical example, analysis[33] of the cyclic voltammetric anodic responses exhibited by **[1A]PF$_6$** with scan rates varying from 0.02 to 1.00 V s$^{-1}$ shows that (a) the current ratio $i_{pc}/i_{pa}$ is constantly equal to 1; (b) the current function $i_{pa}/v^{1/2}$ remains constant; (c) the peak-to-peak separation does not depart appreciably from the theoretically expected value of 59 mV for a chemically and electrochemically reversible one-electron step. The same diagnostic criteria hold for the first reduction step, even if exhaustive electrolysis proved that the full chemical reversibility is limited to the cyclic voltammetric time scale (some tenths of seconds). The electrochemical reversibility of both redox processes indicates that any structural reorganizations accompanying the electron transfer must be fast and reversible.

Of special interest are the voltammetric profiles of the multielectron reductions in DMF solutions of **[2A](PF$_6$)$_2$** and **[4A](PF$_6$)$_4$**. In the case of **[2A](PF$_6$)$_2$**, the peak-to-peak separation of the two overlapping one-electron additions occurring at the first ($\Delta E_p$ = 90 mV) and the second step ($\Delta E_p$ = 96 mV) approaches that of a one-electron transfer (**[1A]PF$_6$**, 66 and 70 mV, respectively). On the other hand, the sequential four-electron additions in each of the two reduction steps of **[4A](PF$_6$)$_4$** appear to be slightly separated but are still essentially overlapping. From a speculative viewpoint, the peak-to-peak separation of about 90 mV for the reduction steps of **[2A](PF$_6$)$_2$** allows the degree of interaction between the two [B(Me)bipy]$^+$ fragments to be evaluated.[34] A comproportionation constant $K_{com}$ of about 10 can be calculated, which does not depart appreciably from the $K_{com}$ value of 4 computed for non-interacting sites. These data suggest, however, that the ferrocene core allows minor electronic communication among the different 2,2′-bipyridylboronium substituents. For a detailed discussion of the propensity of a sandwich complex spacer to promote electronic communication between peripheral groups, the reader is referred to studies of Elschenbroich et al.[35-37]

Finally, the 1,10-phenanthroline complex **[1E]PF$_6$** exhibits the usual one-electron oxidation centered on the ferrocene backbone, but at variance with the corresponding 2,2′-bipyridine complex **[1A]PF$_6$**, it gives rise to two irreversible one-electron reductions both in CH$_2$Cl$_2$ as well as in DMF solution.

---

(31) Allen, F. H.; Kennard, O.; Taylor, R. *Acc. Chem. Res.* **1983**, *16*, 146.

(32) Murata, S.; Mori, T.; Oki, M. *Bull. Chem. Soc. Jpn.* **1984**, *57*, 1970.

(33) Brown, E. R.; Sandifer, J. In *Physical Methods in Chemistry. Electrochemical Methods*; Rossiter, B. W., Hamilton, J. F., Eds.; Wiley: New York, 1986.

(34) Richardson, D. E.; Taube, H. *Inorg. Chem.* **1981**, *20*, 1278.

(35) Elschenbroich, C.; Bilger, E.; Heck, J.; Stohler, F.; Heinzer, J. *Chem. Ber.* **1984**, *117*, 23.

(36) Elschenbroich, C.; Hoppe, S.; Metz, B. *Chem. Ber.* **1993**, *126*, 399.

(37) Elschenbroich, C.; Kühlkamp, P.; Koch, J.; Behrendt, A. *Chem. Ber.* **1996**, *129*, 871.

**Table 3. Formal Electrode Potentials (V *vs* SCE) and Peak-to-Peak Separations (mV, at 0.2 Vs$^{-1}$) for the Redox Changes Exhibited by the Present Ferrocene Derivatives, Together with Wavelengths (nm) for the Oxidized Ferricinium Species**

| | $E^{\circ\prime}_{\text{red1}}$ ($\Delta E_p$) | $E^{\circ\prime}_{\text{red2}}$ ($\Delta E_p$) | $E^{\circ\prime}_{\text{ox}}$ ($\Delta E_p$) | $\lambda_{\max}$ | solvent |
|---|---|---|---|---|---|
| **[1A]PF$_6$** | −1.02 (66) | −1.71 (70) | +0.40 (66) | 626 | DMF |
| | −0.99 (74) | −1.79[a] | +0.42 (68) | | CH$_2$Cl$_2$ |
| **[1C]PF$_6$** | −0.88 (60) | −1.54 (63) | +0.43 (60) | 625 | DMF |
| | −0.87 (68) | −1.72[a] | +0.41 (75) | | CH$_2$Cl$_2$ |
| **[1D]PF$_6$** | −0.99 (60) | −1.68[a] | +0.41 (59) | 625 | DMF |
| | −0.98 (80) | −1.77[a] | +0.43 (78) | | CH$_2$Cl$_2$ |
| **[1E]PF$_6$** | −0.99[a] | −1.80[a] | +0.37 (68) | 627 | DMF |
| | −0.96[a] | | +0.42 (78) | | CH$_2$Cl$_2$ |
| **[2A](PF$_6$)$_2$** | −0.98 (90) | −1.71 (96) | +0.43 (76) | 637 | DMF |
| | −1.00 (89) | −1.82[a] | +0.41 (63) | | CH$_2$Cl$_2$ |
| **[4A](PF$_6$)$_4$** | −1.05[b] | −1.85[b] | +0.38 (70) | 660 | DMF |
| | −1.05[b] | | +0.41 | | CH$_2$Cl$_2$[c] |
| **FcH** | | | +0.49 (72) | | DMF |
| | | | +0.44 (90) | 620 | CH$_2$Cl$_2$ |
| **[1J]PF$_6$** | −0.87 (68) | −1.56 (68) | | | DMF |

[a] Peak potential value, measured at 0.2 V s$^{-1}$. [b] Averaged value between the most cathodic and the most anodic peaks. [c] Essentially insoluble.

Table 3 summarizes the electrochemical parameters of the redox changes exhibited by the ferrocene derivatives under investigation, together with the spectrophotometric characteristics of the corresponding ferricinium congeners in the visible region of the electronic spectrum.

Despite their positive formal charge, the tetracoordinated boron substituents appear to act as weak electron donors toward the ferrocene unit, thereby shifting its oxidation potential to somewhat less positive values compared to unsubstituted ferrocene. Most importantly, the effect of substituents at boron on the oxidation potentials of complexes **[1A]PF$_6$**, **[1C]PF$_6$**, and **[1D]PF$_6$** is surprisingly small (Table 3). This further testifies that the electron is removed from an essentially metallic HOMO level. Also somewhat surprising is the fact that no electrostatic repulsion affects the oxidation potential of the tetracation **[4A]$^{4+}$** to the corresponding pentacation **[4A]$^{5+}$**, likely because a high degree of charge delocalization within the B(Me)bipy moieties is operative. The differences in reduction potentials of complexes **[1A,C,D]PF$_6$** are also quite small and basically reflect the different electronegativities of the substituents at boron.

**Indications for Donor−Acceptor Interactions in [1A]$^+$, [2A]$^{2+}$, and [4A]$^{4+}$.** As outlined above, the ferrocene-based 2,2′-bipyridylboronium ions possess an intense purple color in solution. Small but significant shifts of the absorption maxima occur when the solvent is changed from acetonitrile to water, whereas the nature of the counteranion employed (Br$^-$, PF$_6^-$) has only a negligible influence on the $\lambda_{\max}$ values (Table 4).

The extinction coefficients $\epsilon$ are found to rise remarkably when additional B(Me)bipy substituents are fixed at the ferrocene backbone (CH$_3$CN; **[1A]PF$_6$**, $\epsilon$ = 480 000 cm$^2$/mol; **[2A](PF$_6$)$_2$**, $\epsilon$ = 870 000 cm$^2$/mol; **[4A](PF$_6$)$_4$**, $\epsilon$ = 1 700 000 cm$^2$/mol). In the crystalline state, **[1A]PF$_6$**, **[2A](PF$_6$)$_2$**, and **[4A](PF$_6$)$_4$** are almost black. This color is unusual for ferrocene derivatives and may originate from three possible chromophores: (i) the B(Me)bipy fragment on its own, (ii) the ferrocene backbone, whose absorptions might have been shifted into the observed region due to inductive effects of the cationic substituents,[38−40] (iii) a charge transfer from orbitals of the ferrocene donor into the $\pi$ system of the electron-poor B(Me)bipy substituent(s).

**Table 4. Absorption Maxima $\lambda$ (nm) and Extinction Coefficients $\epsilon$ (1000 cm$^2$ mol$^{-1}$) of [1A]X, [2A]X$_2$, and [4A](PF$_6$)$_4$ in the Visible Region of the Electronic Spectrum**

| | $\lambda_{\max}$ | $\epsilon$ | solvent |
|---|---|---|---|
| **[1A]PF$_6$** | 508 | 480 | CH$_3$CN |
| **[1A]Br** | 502 | 520 | CH$_3$CN |
| **[1A]Br** | 496 | 370 | H$_2$O |
| **[2A](PF$_6$)$_2$** | 514 | 870 | CH$_3$CN |
| **[2A]Br$_2$** | 514 | 890 | CH$_3$CN |
| **[2A]Br$_2$** | 496 | 700 | H$_2$O |
| **[4A](PF$_6$)$_4$** | 540 | 1700 | CH$_3$CN |

2,2′-Bipyridylboronium salts may be colored for various reasons: *Inter*molecular charge-transfer (CT) interactions between cations **[I]$^+$** (Figure 1) and, e.g., iodide counterions, which usually give rise to a yellow color, have been described already in the very first reports on this class of compounds.[41] Moreover, derivatives [R$_2$Bbipy]$^+$ (R = NR$_2$′, OR′, halogen) sometimes show a red color, resulting from an *intra*molecular CT process between the electron lone pairs of the substituents R and the aromatic system.[41] Neither the PF$_6^-$ counterion nor the methyl group possesses polarizable $\pi$ electrons, therefore, similar effects are certainly not operative in **[1A]PF$_6$**, **[2A](PF$_6$)$_2$**, and **[4A](PF$_6$)$_4$**. Moreover, **[1J]X** (Figure 6), which we will use as a model system for the hypothetical iron-free analogue of **[1A]PF$_6$**, is a white solid forming colorless acetonitrile solutions. Boron coordination obviously does not decrease the energy of the $\pi \rightarrow \pi^*$ transition within the aromatic ligand to a sufficiently great extent to cause light absorption in the visible region of the electronic spectrum. We may, therefore, conclude that the B(Me)bipy substituent alone is not the chromophore in compounds **[1A]PF$_6$**, **[2A](PF$_6$)$_2$**, and **[4A](PF$_6$)$_4$**.

To investigate only the inductive effects of cationic boronium substituents on the UV−vis spectral data of the ferrocene unit and to separate them from other electronic influences that might arise from the special features of the B(Me)bipy system, we have prepared the $\gamma$-picoline derivative **[1G]Br** (Figure 2). **[1G]$^+$** is very similar to **[1A]$^+$** except that the carbon−carbon bridge connecting both pyridine rings is missing. This modification should largely eliminate the electron-accepting ability of the amine ligands, which is dependent on the presence of an extended $\pi$-system being able to adopt quinoid character in the reduced form(s) (Figure 1). On the other hand, the nature of the boronium cation attached to the ferrocene core is changed as little as possible, thereby ensuring only minor changes of its substituent effects on the ferrocene core. **[1G]Br** was found to be a pale yellow compound both in the solid state and in solution ($\lambda_{\max}$ = 448 nm; acetonitrile) and, thus, possesses the usual color of ferrocenyl fragments bearing tetracoordinate boron centers.[12,19] Therefore, the color of **[1A]PF$_6$**, **[2A](PF$_6$)$_2$**, and **[4A](PF$_6$)$_4$** is probably not caused by a shift in energy of either a Fe-

---

(38) Hennig, H.; Gürtler, O. *J. Organomet. Chem.* **1968**, *11*, 307.

(39) Sohn, Y. S.; Hendrickson, D. N.; Gray, H. B. *J. Am. Chem. Soc.* **1971**, *93*, 3603.

(40) Zerner, M. C.; Loew, G. H.; Kirchner, R. F.; Mueller-Westerhoff, U. T. *J. Am. Chem. Soc.* **1980**, *102*, 589.

(41) Banford, L.; Coates, G. E. *J. Chem. Soc.* **1964**, 3564.

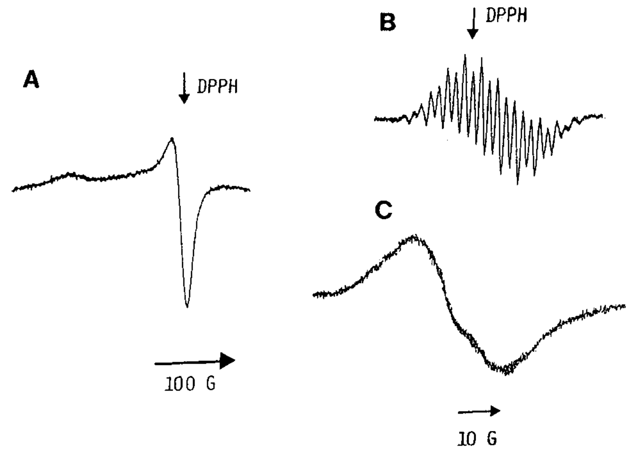

**Figure 8.** X-band ESR spectra recorded on DMF solutions of electrogenerated **[1A]$^0$**. (a, c) T = 100 K, (b) T = 260 K.

to-Cp MLCT or a d → d transition within the ferrocene core. To obtain purple colored salts, *both* the ferrocene donor *and* an intact B(R)bipy acceptor have to be present at the same time. As could be expected from the rather poor match of the redox potentials of ferrocene ($E^{\circ\prime}_{+/0}$ = 0.49 V *vs* SCE; DMF solution) and, e.g., **[1J]PF$_6$** ($E^{\circ\prime}_{+/0}$ = −0.87 V *vs* SCE; DMF solution), no color change is observed upon mixing acetonitrile solutions of both molecules. The close contact between donor and acceptor established in **[1A]PF$_6$**, **[2A](PF$_6$)$_2$**, and **[4A](PF$_6$)$_4$**, thus, appears to be a second prerequisite for the CT process to occur. It is noteworthy in this context that a bright green color has been observed for inclusion complexes of square cyclophanes made up of two 4,4′-bipyridinium units and two hydrochinone rings with ferrocene as the guest molecule. This phenomenon has also been attributed to CT interactions between the electron-rich sandwich compound and the electron-poor bipyridinium rings.[42]

In an attempt to ascertain whether the ferrocene backbone might contribute to the character of the LUMO level of **[1A]PF$_6$**, we decided to record the X-band ESR spectrum of the one-electron reduced congener **[1A]$^0$** at $T$ = 100 K. Because of the marked sensitivity of this radical toward traces of air and moisture (see above), **1A$^0$** was electrogenerated by controlled-potential electrolysis at 253 K in order to slow down its decomposition rate. Figure 8a shows the axial signal ($g_{||} > g_{\perp} > g_e = 2.0023$) obtained upon immediate freezing of the sample at liquid nitrogen temperature. The anisotropic line shape is typical of a $S = {}^1/_2$ paramagnetic species displaying some metal-in character ($g_{||}$ = 2.090(8), $g_{\perp}$ = 2.004(8), $\langle g \rangle$ = 2.032(8)) without any detectable hyperfine (hpf) resolution.

Since it is well-conceivable that the added electron enters mainly the aromatic bipy framework (see above), we interpret the unusual features of the ESR resonance as due to orbital overlap between the central iron atom (3d orbitals) and the B(Me)bipy substituent ($\pi$ orbitals). In agreement with the chemical reversibility of the electron transfer, no significant change in the spectral pattern was observed upon freezing samples withdrawn either at the first stages of the electrolysis or after exhaustive one-electron reduction. No changes in the redox pattern of the **[1A]$^+$** / **[1A]$^0$** couple takes place in the long times of electrolysis, except for the progressive passing from a reduction to an oxidation process.

At the glassy−fluid transition, the initially observed ESR signal drops out while concomitantly a narrow and isotropic signal builds up centered at $g_{iso}$(260 K) = 2.000(5), which then rapidly and irreversibly vanishes. In contrast, when **[1A]$^0$** is placed into the resonance cavity at $T$ = 253 K, a narrow and complex isotropic ESR signal arises at $g_{iso}$(260 K) = 2.0012(8), which is typical of an organic radical species (Figure 8b). The partially resolved spectral pattern displays 21 detectable lines spaced by 2.0 G, likely resulting from the hpf coupling of the unpaired electron with the magnetically active bipy atoms ($I_N = 1$; $I_H = {}^1/_2$). The relevant liquid-nitrogen spectrum shown in Figure 8c exhibits paramagnetic features consistent with those of the fluid solution ($g_{av}$ = 2.0024(8)) but differing from the glassy metal-centered species.

Such spectral behavior again suggests that the reduced species **[1A]$^0$**, which is rather stable within the electrolysis cell under inert atmosphere, is sensitive to traces of dioxygen or water, which lead to C−B bond cleavage. As a further confirmation of this interpretation, samples from the one-electron exhaustive reduction of **[1J]PF$_6$** at 260 K afford a well-resolved multiline spectrum ($g_{iso}$ = 2.0012(8)) quite coincident with that of the radical species shown in Figure 8b.

Table 5 summarizes the X-band ESR parameters of the paramagnetic species **[1A]$^0$**, **[1C]$^0$**, **[1D]$^0$**, **[2A]$^0$**, and **[4A]$^0$**. Under glassy conditions, only **[1A]$^0$**, **[1C]$^0$**, and **[2A]$^0$** displayed the above-mentioned signal having metallic character, whereas at 260 K all the reduction products exhibited the typical organic pattern, except of **[4A]$^0$**, which was not detected.

**Quantum Chemical Calculations.** To gain further insight into the charge density distribution of a 2,2′-bipyridylboronium cation, as well as the radical and the anion obtained upon reduction, we have performed MNDO calculations on the model system [Me$_2$Bbipy]$^{+/0/-}$ **[1K]$^{+/0/-}$** (symmetry point group $C_s$) using the AM1 program package[43] (Figure 6). The optimized molecular geometries, together with the Mulliken charges on the heavy atoms, are summarized in Tables 6 and 7 and compared with the free ligand 2,2′-bipyridine in its *Z* conformation.

The calculated molecular structure of **[1K]$^+$** is in reasonable agreement with the one found for the B(Me)bipy substituents in **[1A]PF$_6$**, **[2A](PF$_6$)$_2$**, and **[4A](PF$_6$)$_4$**. The largest deviation between theory, which represents isolated molecules in the gas phase, and experiment is found for the B−N bond lengths (mean value in **[1A]PF$_6$**, **[2A](PF$_6$)$_2$**, and **[4A](PF$_6$)$_4$**, 1.597 Å; **[1K]$^+$**, 1.662 Å). This effect is generally observed with dative bonds and has to be attributed to their high polarity, which leads to a contraction of bond lengths in the crystal lattice due to dipole−dipole interactions.[28]

Characteristic changes of the calculated geometries are observed upon going from the cationic **[1K]$^+$** to the uncharged radical **[1K]$^0$** and the anionic **[1K]$^-$**: N−C2 and C2−C3 are elongated by 0.047 and 0.050 Å (see Figure 1 for the numbering scheme). In contrast, the overall bond lengths C2−C2′, C3−C4, and C5−C6

---

(42) Ashton, P. R.; Claessens, C. G.; Hayes, W.; Menzer, S.; Stoddart, J. F.; White, A. J. P.; Williams, D. J. *Angew. Chem.* **1995**, *107*, 1994; *Angew. Chem., Int. Ed. Engl.* **1995**, *34*, 1862.

(43) Stewart, J. J. P. *program MOPAC, version 6.0*; **1990**.

**Table 5. X-Band ESR Parameters Exhibited by the Present Ferrocene Molecules upon Cathodic Reduction at 253 K at the First Reduction Process in DMF Solution**

| | metal-centered radical | | | | organic radical | | |
|---|---|---|---|---|---|---|---|
| | $g_{\|\|}$[a] | $g_{\perp}$[a] | $<g>$[a,b] | $g_{av}$[a] | $g_{iso}$[c] | hpf splitting (G)[c] | lines[c] |
| **[1A]$^0$** | 2.090(8) | 2.004(8) | 2.032(8) | 2.0024(8) | 2.0012(8) | 2.0 (5) | 21 |
| **[1C]$^0$** | 2.046(8) | 2.004(8) | 2.018(8) | 2.001(5) | 1.998(5) | 2.5 (8) | 13 |
| **[1D]$^0$** | | | | 2.001(8) | 2.0012(8) | 2.5 (8) | 15 |
| **[2A]$^0$** | 2.051(8) | 2.004(8) | 2.020(8) | 2.0054(8) | 2.0054(8) | 2.0 (5) | 13 |
| **[4A]$^0$** | | | | 2.004(5) | | | |

[a] $T = 100$ K. [b] $<g> = {}^1/_3\,(g_{\|\|} + 2g_{\perp})$. [c] $T = 260$ K.

**Table 6. Calculated Bond Lengths (Å) and Angles (deg) of $[\mathbf{1K}]^{+/0/-}$ Compared to 2,2′-Bipyridine (bipy)**

| | **[1K]$^+$** | **[1K]$^0$** | **[1K]$^-$** | bipy |
|---|---|---|---|---|
| B−N | 1.662 | 1.629 | 1.597 | |
| N−C2 | 1.384 | 1.399 | 1.431 | 1.363 |
| C2−C3 | 1.394 | 1.426 | 1.444 | 1.414 |
| C3−C4 | 1.407 | 1.380 | 1.362 | 1.397 |
| C4−C5 | 1.391 | 1.411 | 1.428 | 1.392 |
| C5−C6 | 1.415 | 1.405 | 1.391 | 1.408 |
| C6−N | 1.341 | 1.344 | 1.339 | 1.341 |
| C2−C2′ | 1.483 | 1.427 | 1.385 | 1.493 |
| N−B−N′ | 96.8 | 97.9 | 99.4 | |
| B−N−C2 | 110.4 | 109.4 | 108.8 | |
| N−C2−C2′ | 111.2 | 111.6 | 111.6 | 118.7 |
| C3−C2−C2′ | 127.0 | 128.0 | 129.9 | 120.0 |

**Table 7. Calculated Partial Electronic Charges of $[\mathbf{1K}]^{+/0/-}$ Compared to 2,2′-Bipyridine (bipy)**

| | **[1K]$^+$** | **[1K]$^0$** | **[1K]$^-$** | **bipy** |
|---|---|---|---|---|
| B | +0.220 | +0.190 | +0.182 | |
| N | −0.084 | −0.104 | −0.198 | −0.098 |
| C2 | +0.019 | −0.041 | −0.060 | +0.029 |
| C3 | −0.108 | −0.159 | −0.188 | −0.171 |
| C4 | −0.047 | −0.072 | −0.077 | −0.099 |
| C5 | −0.140 | −0.237 | −0.403 | −0.175 |
| C6 | +0.015 | +0.008 | +0.070 | −0.072 |
| $CH_3$ | −0.296 | −0.283 | −0.277 | |

become shorter by 0.098, 0.045, and 0.024 Å, respectively. This observation is in accord with the assumption of a largely aromatic π-system in **[1K]**$^+$ and a quinoid structure with more localized single and double bonds in **[1K]**$^-$. Significantly shorter B−N bonds are found in the fully reduced anion ($d_{BN} = 1.597$ Å) than in the corresponding cation ($d_{BN} = 1.662$ Å). Consequently, the positive partial charge on the boron center decreases from **[1K]**$^+$ (+0.220) to **[1K]$^0$** (+0.190) and **[1K]**$^-$ (+0.182). However, these changes are only modest, thus, testifying to the fact that the electronic charge of **[1K]**$^+$ and **[1K]**$^-$ is mainly located at the aromatic ligand. As outlined above, this interpretation is supported by the X-ray crystallographic data of **[1A]PF$_6$**, **[2A](PF$_6$)$_2$**, and **[4A](PF$_6$)$_4$**. Upon reduction of **[1K]**$^+$, the nitrogen centers and the carbon atoms in positions 3 and 5 of the bipy donor are the major sites of charge accumulation (Table 7). In view of the theoretical data at hand, it seems more appropriate to consider compounds like $[R_2Bbipy]^+$ as bipyridinium borates rather than bipyridine boronium salts. This is also in agreement with the experimental finding of slightly less anodic Fe(II)/Fe(III) oxidation potentials in **[1A]PF$_6$**, **[2A](PF$_6$)$_2$**, and **[4A](PF$_6$)$_4$** compared to the parent ferrocene molecule. This effect can easily be explained by some inductive charge donation from the tetracoordinate boron atoms, which is not outweighted by the ferrocene-to-bipy CT process.

## Conclusion

A high-yield synthesis of donor−acceptor complexes **[1A−D]X**, **[2A]X$_2$**, and **[4A]X$_4$** with one, two, and four $[B(R)bipy]^+$ acceptors (R = Me, Br, OEt, $NC_4H_8$; X = Br, $PF_6$) covalently attached to a ferrocene donor has been described. From the viewpoint of synthesis, our approach benefits from the spontaneous formation of dative boron−nitrogen bonds, which switch on the acceptor unit by polarizing the electron cloud of the 2,2′-bipyridine ligand and at the same time link together the donor and acceptor functionalities.

In DMF solution and under an inert atmosphere, **[1A]PF$_6$**, **[1C]PF$_6$**, **[1D]PF$_6$**, **[2A](PF$_6$)$_2$**, and **[4A](PF$_6$)$_4$** behave as reversible three-step redox systems capable of storing three, five, and nine electrons, respectively. The effect of substituents R at boron on the respective redox potentials appears to be rather limited. Moreover, the potential of the Fe(II)/Fe(III) redox transition is almost unaffected by the number of B(Me)bipy substituents attached to the ferrocene core. There is evidence for a weak electronic interaction between the individual B(Me)bipy units in **[2A](PF$_6$)$_2$** and **[4A](PF$_6$)$_4$**.

The complexes **[1A−F]X**, **[2A]X$_2$**, and **[4A]X$_4$** possess an intense purple color both in solution and in the solid state. It was shown for **[1A]PF$_6$**, **[2A](PF$_6$)$_2$**, and **[4A](PF$_6$)$_4$** that the extinction coefficients of the corresponding absorptions in the visible region of the electronic spectrum correlate with the number of pendant B(Me)bipy units. If in **[1A]**$^+$ the conjugated bifunctional ligand 2,2′-bipyridine is replaced by 2 equiv of the monobasic γ-picoline, the resulting complex **[1G]**$^+$ not only possesses a lower stability toward hydrolysis but also the color changes from purple to pale yellow. When the colorless boronium salt **[1J]PF$_6$** is added to a yellow acetonitrile solution of ferrocene, no significant additional bands are observed in the visible electronic spectrum. We, therefore, conclude that the intense color of, for example, **[1A]PF$_6$**, **[2A](PF$_6$)$_2$**, and **[4A](PF$_6$)$_4$** is not due to bipy-based chromophores only but to a charge-transfer process between the ferrocene backbone and the B(Me)bipy units, which depends on (i) the presence of a conjugated elctron-poor π-system and (ii) the close contact between donor and acceptor. This interpretation is supported by the ESR spectrum of the neutral radical **[1A]$^0$**, which gives evidence for admixture of ligand and metal orbitals to the SOMO of the donor−acceptor complex. The type of Fe-to-bipy charge-transfer is, thus, reminiscent of Fe−B and Fe−$C_{exo}$ interactions in **1b** and ferrocene-stabilized carbonium ions ($[FcCR_2]^+$).[44]

We would like to underline that **[4A](PF$_6$)$_4$**, being able to reversibly tolerate the loss of one electron, as

---

[44] Appel, A.; Jäkle, F.; Priermeier, T.; Schmid, R.; Wagner, M. *Organometallics* **1996**, *15*, 1188 and references cited therein.

well as the addition of eight electrons, is among those molecules exhibiting the largest redox aptitude.[45−47] Work is in progress in our laboratory to incorporate these highly efficient electron sponges into linear (**[2A](PF$_6$)$_2$**) and dendritic (**[4A](PF$_6$)$_4$**) macromolecules by using 2,2′-bipyridine derivatives with polymerizable side chains. Another successful synthesis strategy is based on the alcoholysis reaction outlined in Scheme 2, which provides a way of connecting ferrocene derivatives bearing more than one B(Br)bipy substituent with bifunctional alcohols.

## Experimental Section

**General Considerations.** All reactions and manipulations of air-sensitive compounds were carried out in dry, oxygen-free argon using standard Schlenk ware or in an argon-filled drybox. Solvents were freshly distilled under $N_2$ from Na/K alloy−benzophenone (toluene, hexane) or from $CaH_2$ ($CH_2Cl_2$, $CH_3CN$) prior to use. NMR: Jeol JMN-GX 400, Bruker DPX 400. $^{11}$B NMR spectra are reported relative to external $BF_3 \cdot Et_2O$. Unless stated otherwise, all NMR spectra were run at ambient temperature; abbreviations: s = singlet; d = doublet; tr = triplet; vtr = virtual triplet; q = quartet; br = broad; mult = multiplet; n.r. = multiplet expected in the $^1$H NMR spectrum but not resolved; n.o. = signal not observed; bipy = 2,2′-bipyridine; phen = 1,10-phenanthroline; bipm = 2,2′-bipyrimidine; pic = $\gamma$-picoline; the numbering of the chelating amines follows the numbering scheme given in Scheme 1 and Figures 1 and 2. Elemental analyses: Microanalytical laboratory of the Technische Universität München. The compounds **1a**−**d**,[18,19] **[1J]PF$_6$**,[41] **2a**,[20] and **4a**[21] were synthesized according to literature procedures.

**Synthesis of [1A]PF$_6$.** A toluene (20 mL) solution of **1a** (1.37 g, 4.71 mmol) was added dropwise with stirring at −60 °C to a solution of 2,2′-bipyridine (0.74 g, 4.74 mmol) in 40 mL of toluene. The mixture instantaneously adopted a blue color, and a blue precipitate gradually formed upon warming to ambient temperature. The slurry was stirred for 5 h, and the solid **[1A]Br** was collected on a frit, extracted with toluene (2 × 20 mL) and hexane (10 mL), and dried *in vacuo*. **[1A]Br** was dissolved in 30 mL of water and the clear purple solution added dropwise at ambient temperature to an aqueous solution of $NH_4PF_6$ (1.63 g, 10.00 mmol), whereupon **[1A]PF$_6$** precipitated quantitatively. Deep purple X-ray quality crystals were grown by layering an acetonitrile solution of **[1A]PF$_6$** with diethyl ether. Yield: 2.24 g (93%).

$^{11}$B NMR (128.3 MHz, $CD_3CN$): $\delta$ 8.6 ($h_{1/2}$ = 140 Hz). $^1$H NMR (400.0 MHz, $CD_3CN$): $\delta$ 0.61 (s, 3H, $CH_3$), 3.81 (vtr, 2H, $^3J$(HH) = $^4J$(HH) = 1.8 Hz, $C_5H_4$), 4.07 (s, 5H, $C_5H_5$), 4.21 (vtr, 2H, $^3J$(HH) = $^4J$(HH) = 1.8 Hz, $C_5H_4$), 8.09 (vtr, 2H, $^3J$(HH) = 5.5 Hz, bipy-5,5′), 8.58 (vtr, 2H, $^3J$(HH) = 7.5 Hz, bipy-4,4′), 8.66 (d, 2H, $^3J$(HH) = 8.0 Hz, bipy-3,3′), 8.97 (d, 2H, $^3J$(HH) = 5.5 Hz, bipy-6,6′). $^{13}$C NMR (100.6 MHz, $CD_3CN$): $\delta$ 7.8 (br, $CH_3$), 69.0 ($C_5H_5$), 70.6, 70.9 ($C_5H_4$), n.o. ($C_5H_4$-*ipso*), 123.7 (bipy-3,3′), 129.4 (bipy-5,5′), 144.1 (bipy-6,6′), 145.2 (bipy-4,4′), 146.0 (bipy-2,2′). Anal. Calcd for $C_{21}H_{20}BF_6FeN_2P$ (512.02): C, 49.26; H, 3.94; Fe, 10.91; N, 5.47. Found: C, 49.32; H, 4.00; Fe, 10.87; N, 5.34.

**Synthesis of [1B]Br.** A solution of **1b** (0.45 g, 1.27 mmol) in 25 mL of $CH_2Cl_2$ was added dropwise with stirring at −78 °C to a solution of 2,2′-bipyridine (0.21 g, 1.34 mmol) in 25 mL of $CH_2Cl_2$. The reaction mixture instantaneously adopted a deep blue color. The solution was allowed to warm to ambient temperature and stirred for 3 h. After filtration from a small amount of insoluble material, the filtrate was treated with 15 mL of hexane, whereupon a dark green-blue microcrystalline solid precipitated. The crude **[1B]Br** was collected on a frit, extracted with hexane/$CH_2Cl_2$ (1:1) and pure hexane, and dried *in vacuo*. Due to its sensitivity to moisture, **[1B]Br** was not transformed into **[1B]PF$_6$**. Yield: 0.59 g (91%).

$^{11}$B NMR (128.3 MHz, $CD_3CN$): $\delta$ 6.8 ($h_{1/2}$ = 150 Hz). $^1$H NMR (400.0 MHz, $CD_3CN$): $\delta$ 4.07 (vtr, 2H, $^3J$(HH) = $^4J$(HH) = 1.8 Hz, $C_5H_4$), 4.11 (s, 5H, $C_5H_5$), 4.36 (vtr, 2H, $^3J$(HH) = $^4J$(HH) = 1.8 Hz, $C_5H_4$), 8.23 (mult, 2H, bipy-5,5′), 8.75 (vtr, 2H, $^3J$(HH) = 7.9 Hz, bipy-4,4′), 8.97 (d, 2H, $^3J$(HH) = 7.9 Hz, bipy-3,3′), 9.23 (d, 2H, $^3J$(HH) = 5.5 Hz, bipy-6,6′). $^{13}$C NMR (100.6 MHz, $CD_3CN$): $\delta$ 69.9 ($C_5H_5$), 71.8, 72.4 ($C_5H_4$), n.o. ($C_5H_4$-*ipso*), 125.1 (bipy-3,3′), 130.8 (bipy-5,5′), 145.1 (bipy-6,6′), 145.2 (bipy-2,2′), 147.7 (bipy-4,4′). Anal. Calcd for $C_{20}H_{17}BBr_2FeN_2$ (511.84): C, 46.93; H, 3.35; N, 5.47. Found: C, 47.45; H, 3.86; N, 5.26.

**Synthesis of [1C]PF$_6$. Method 1: [1C]PF$_6$** was synthesized similar to **[1A]PF$_6$** from **1c** (0.75 g, 2.34 mmol), 2,2′-bipyridine (0.36 g, 2.30 mmol), and $NH_4PF_6$ (0.82 g, 5.03 mmol). Yield: 1.16 g (93%).

$^{11}$B NMR (128.3 MHz, $CD_3CN$): $\delta$ 10.8 ($h_{1/2}$ = 160 Hz). $^1$H NMR (400.0 MHz, $CD_3CN$): $\delta$ 1.06 (tr, 3H, $^3J$(HH) = 7.3 Hz, $OCH_2CH_3$), 3.08 (q, 2H, $^3J$(HH) = 7.3 Hz, $OCH_2CH_3$), 3.88 (n.r., 2H, $C_5H_4$), 3.92 (s, 5H, $C_5H_5$), 4.20 (n.r., 2H, $C_5H_4$), 8.14 (mult, 2H, bipy-5,5′), 8.65 (mult, 4H, bipy-3,3′,4,4′), 8.97 (d, 2H, $^3J$(HH) = 5.5 Hz, bipy-6,6′). $^{13}$C NMR (100.6 MHz, $CD_3CN$): $\delta$ 18.0 ($OCH_2CH_3$), 59.7 ($OCH_2CH_3$), 69.4 ($C_5H_5$), 70.9, 71.9 ($C_5H_4$), n.o. ($C_5H_4$-*ipso*), 124.1 (bipy-3,3′), 130.1 (bipy-5,5′), 144.8 (bipy-6,6′), 145.6 (bipy-2,2′), 146.8 (bipy-4,4′). Anal. Calcd for $C_{22}H_{22}BF_6FeN_2OP$ (542.05): C, 48.75; H, 4.09; N, 5.17. Found: C, 48.16; H, 4.08; N, 4.88.

**Method 2: [1B]Br** (90 $\mu$g, 180 $\mu$mol) was treated at ambient temperature with a mixture of EtOH (3 mL) and $NEt_3$ (26 $\mu$L, 19 $\mu$g, 190 $\mu$mol). A clear purple solution was obtained, which was stirred for 1 h and then evaporated to dryness *in vacuo*. The solid purple residue of **[1C]Br** was treated with $CH_2Cl_2$ (2 × 5 ml), dissolved in 10 mL of water, and precipitated in almost quantitative yield as its $PF_6$ salt. All NMR spectra are identical with those of the product obtained from method 1.

**Synthesis of [1D]PF$_6$. [1D]PF$_6$** was synthesized similar to **[1A]PF$_6$** from **1d** (0.90 g, 2.60 mmol), 2,2′-bipyridine (0.41 g, 2.63 mmol), and $NH_4PF_6$ (0.90 g, 5.52 mmol). Yield: 1.33 g (90%).

$^{11}$B NMR (128.3 MHz, $CD_3CN$): $\delta$ 10.6 ($h_{1/2}$ = 150 Hz). $^1$H NMR (400.0 MHz, $CD_3CN$): $\delta$ 1.66 (n.r., 4H, $NCH_2CH_2$), 2.69 (tr, 4H, $^3J$(HH) = 6.1 Hz, $NCH_2CH_2$), 3.61 (s, 5H, $C_5H_5$), 3.87, 4.23 (2 × n.r., 2 × 2H, $C_5H_4$), 8.11 (vtr, 2H, $^3J$(HH) = 5.5 Hz, bipy-5,5′), 8.62 (vtr, 2H, $^3J$(HH) = 7.3 Hz, bipy-4,4′), 8.72 (d, 2H, $^3J$(HH) = 7.3 Hz, bipy-3,3′), 8.90 (d, 2H, $^3J$(HH) = 5.5 Hz, bipy-6,6′). $^{13}$C NMR (100.6 MHz, $CD_3CN$): $\delta$ 27.1 ($NCH_2CH_2$), 48.0 ($NCH_2CH_2$), 68.8 ($C_5H_5$), 70.6, 71.9 ($C_5H_4$), n.o. ($C_5H_4$-*ipso*), 123.6 (bipy-3,3′), 129.6 (bipy-5,5′), 144.7 (bipy-6,6′), 145.2 (bipy-2,2′), 145.9 (bipy-4,4′). Anal. Calcd for $C_{24}H_{25}BF_6FeN_3P$ (567.11): C, 50.83; H, 4.44; Fe 9.94; N, 7.41. Found: C, 50.36; H, 4.51; Fe, 9.62; N, 6.99.

**Synthesis of [1E]PF$_6$. [1E]PF$_6$** was synthesized similar to **[1A]PF$_6$** from **1a** (1.06 g, 3.65 mmol), 1,10-phenanthroline (0.66 g, 3.66 mmol), and $NH_4PF_6$ (1.30 g, 7.98 mmol). Yield: 1.66 g (85%).

$^{11}$B NMR (128.3 MHz, $CD_3CN$): $\delta$ 10.8 ($h_{1/2}$ = 140 Hz). $^1$H NMR (400.0 MHz, $CD_3CN$): $\delta$ 0.75 (s, 3H, $CH_3$), 3.91 (n.r., 2H, $C_5H_4$), 4.04 (s, 5H, $C_5H_5$), 4.21 (n.r., 2H, $C_5H_4$), 8.36 (dd, 2H, $^3J$(HH) = 5.5, 8.3 Hz, phen-5,5′), 8.43 (s, 2H, phen-7,7′), 9.10 (d, 2H, $^3J$(HH) = 8.3 Hz, phen-4,4′), 9.28 (d, 2H, $^3J$(HH) = 5.5 Hz, phen-6,6′). $^{13}$C NMR (100.6 MHz, $CD_3CN$): $\delta$ n.o. ($CH_3$), 69.1 ($C_5H_5$), 70.8, 71.3 ($C_5H_4$), n.o. ($C_5H_4$-*ipso*), 128.5, 128.5 (phen-5,5′,7,7′), 129.6 (phen-3,3′), 138.2 (phen-2,2′), 142.4 (phen-6,6′), 144.7 (phen-4,4′). Anal. Calcd for $C_{23}H_{20}BF_6FeN_2P$ (536.05): C, 51.53; H, 3.76; Fe, 10.42; N, 5.23. Found: C, 51.93; H, 4.03; Fe, 10.46; N, 5.08.

---

(45) Fillaut, J.-L.; Linares, J.; Astruc, D. *Angew. Chem.* **1994**, *106*, 2540; *Angew. Chem., Int. Ed. Engl.* **1994**, *33*, 2460.

(46) Jutzi, P.; Batz, C.; Neumann, B.; Stammler, H.-G. *Angew. Chem.* **1996**, *108*, 2272; *Angew. Chem., Int. Ed. Engl.* **1996**, *35*, 2118.

(47) Grossmann, B.; Heinze, J.; Herdtweck, E.; Köhler, F. H.; Nöth, H.; Schwenk, H.; Spiegler, M.; Wachter, W.; Weber, B. *Angew. Chem.* **1997**, *109*, 384; *Angew. Chem., Int. Ed. Engl.* **1997**, *36*, 387.

**Synthesis of [1F]Br. [1F]Br** was synthesized similar to **[1A]Br** from **1a** (0.21 g, 0.72 mmol) and 2,2′-bipyrimidine (0.11 g, 0.70 mmol). Yield: 0.27 g (86%).

$^{11}$B NMR (128.3 MHz, $CD_3CN$): $\delta$ 7.7 ($h_{1/2}$ = 200 Hz). $^{1}$H NMR (400.0 MHz, $CD_3CN$): $\delta$ 0.67 (s, 3H, $CH_3$), 3.90 (n.r., 2H, $C_5H_4$), 4.18 (s, 5H, $C_5H_5$), 4.25 (vtr, 2H, $^3J$(HH) = 1.8 Hz, $C_5H_4$), 8.26 (mult, 2H, bipm-5,5′), 9.35 (dd, 2H, $^3J$(HH) = 6.1 Hz, $^4J$(HH) = 1.8 Hz, bipm-4,4′), 9.59 (dd, 2H, $^3J$(HH) = 4.9 Hz, $^4J$(HH) = 1.8 Hz, bipm-6,6′). $^{13}$C NMR (100.6 MHz, $CD_3CN$): $\delta$ n.o. ($CH_3$), 69.3 ($C_5H_5$), 71.0, 71.5 ($C_5H_4$), n.o. ($C_5H_4$-*ipso*), 126.2 (bipm-5,5′), 151.8 (bipm-4,4′), 153.8 (bipm-2,2′), 166.1 (bipm-6,6′). Anal. Calcd for $C_{19}H_{18}BBrFeN_4$ (448.94): C, 50.83; H, 4.04; N, 12.48. Found: C, 51.05; H, 4.17; N, 12.13.

**Synthesis of [1G]Br. 1a** (0.30 g, 1.03 mmol) was dissolved at ambient temperature in 5 mL of $\gamma$-picoline. The resulting yellow solution was stirred for 12 h, whereupon a yellow precipitate gradually formed. The solid material was collected on a frit, extracted with hexane (5 × 10 mL), and dried *in vacuo*. Due to its sensitivity to moisture, **[1G]Br** was not transformed into **[1G]PF$_6$**. Yield: 0.44 g (89%).

$^{11}$B NMR (128.3 MHz, $CDCl_3$): $\delta$ 6.4 ($h_{1/2}$ = 400 Hz). $^{1}$H NMR (400.0 MHz, $CDCl_3$): $\delta$ 0.81 (s, 3H, $BCH_3$), 2.54 (s, 6H, $CCH_3$), 3.80 (s, 5H, $C_5H_5$), 3.86, 4.28 (2 × n.r., 2 × 2H, $C_5H_4$), 7.67 (d, 4H, $^3J$(HH) = 6.5 Hz, pic-3,5), 8.43 (d, 4H, $^3J$(HH) = 6.5 Hz, pic-2,6). $^{13}$C NMR (100.5 MHz, $CDCl_3$): $\delta$ 9.2 ($BCH_3$), 21.8 ($CCH_3$), 68.1 ($C_5H_5$), 70.6, 71.7 ($C_5H_4$), n.o. ($C_5H_4$-*ipso*), 127.8 (pic-3,5), 144.7 (pic-2,6), 156.5 (pic-4). Anal. Calcd for $C_{23}H_{26}BBrFeN_2$ (477.04): C, 57.91; H, 5.49; Fe 11.71; N, 5.87. Found: C, 58.05; H, 5.70; Fe, 11.74; N, 6.10.

**Synthesis of [2A](PF$_6$)$_2$.** A $CH_2Cl_2$ (30 mL) solution of **2a** (3.02 g, 7.64 mmol) was added dropwise with stirring at −60 °C to a solution of 2,2′-bipyridine (2.39 g, 15.30 mmol) in 40 mL of $CH_2Cl_2$. The mixture instantaneously adopted a purple color, and a purple precipitate gradually formed upon warming to ambient temperature. The slurry was stirred for several hours, and the solid material was collected on a frit and extracted with $CH_2Cl_2$ (3 × 10 mL). **[2A]Br$_2$** was dissolved in 30 mL of water, and the clear purple solution was added dropwise at ambient temperature to an aqueous solution of $NH_4PF_6$ (5.71 g, 35.03 mmol), whereupon **[2A](PF$_6$)$_2$** precipitated quantitatively. Deep purple X-ray quality crystals were grown by layering an acetonitrile solution of **[2A](PF$_6$)$_2$** with diethyl ether. Yield: 5.69 g (89%).

$^{11}$B NMR (128.3 MHz, $CD_3CN$): $\delta$ 8.5 ($h_{1/2}$ = 240 Hz). $^{1}$H NMR (400.0 MHz, $CD_3CN$): $\delta$ 0.49 (s, 6H, $CH_3$), 3.68, 4.02 (2 × n.r., 2 × 4H, $C_5H_4$), 8.07 (vtr, 4H, $^3J$(HH) = 7.0 Hz, bipy-5,5′), 8.58 (vtr, 4H, $^3J$(HH) = 8.0 Hz, bipy-4,4′), 8.66 (d, 4H, $^3J$(HH) = 8.0 Hz, bipy-3,3′), 8.89 (d, 4H, $^3J$(HH) = 6.0 Hz, bipy-6,6′). $^{13}$C NMR (100.6 MHz, $CD_3CN$): $\delta$ 7.7 (br, $CH_3$), 70.9, 71.0 ($C_5H_4$), n.o. ($C_5H_4$-*ipso*), 123.8 (bipy-3,3′), 129.4 (bipy-5,5′), 144.1 (bipy-6,6′), 145.3 (bipy-4,4′), 146.0 (bipy-2,2′). Anal. Calcd for $C_{32}H_{30}B_2F_{12}FeN_4P_2$ (838.02): C, 45.86; H, 3.61; F, 27.20; N, 6.68. Found: C, 45.59; H, 3.50; F, 27.33; N, 6.37.

**Synthesis of [4A](PF$_6$)$_4$.** A $CH_2Cl_2$ (20 mL) solution of **4a** (0.69 g, 1.14 mmol) was added dropwise with stirring at −60 °C to a solution of 2,2′-bipyridine (0.70 g, 4.48 mmol) in 40 mL of $CH_2Cl_2$. The mixture instantaneously adopted a blue color, and a blue precipitate gradually formed upon warming to ambient temperature. The slurry was stirred for 12 h, and the solid material was collected on a frit and extracted with $CH_2Cl_2$ (3 × 10 ml). **[4A]Br$_4$** was dissolved in 30 mL of water, and the clear purple solution was added dropwise at ambient temperature to an aqueous solution of $NH_4PF_6$ (1.63 g, 10.00 mmol), whereupon **[4A](PF$_6$)$_4$** precipitated quantitatively. The compound was purified by recrystallization from $CH_3CN$/diethyl ether. Yield: 1.48 g (85%). Deep purple X-ray quality crystals of **[4A]Br$_4$** were grown by slowly evaporating its ethanol (96%) solution.

$^{11}$B NMR (128.3 MHz, DMSO-$d_8$): $\delta$ 8.5 ($h_{1/2}$ = 500 Hz). $^{1}$H NMR (400.0 MHz, DMSO-$d_8$): $\delta$ 0.27, 0.70 (2 × s, 2 × 6H, $CH_3$), 2.53, 3.24, 4.87 (3 × s, 3 × 2H, $C_5H_3$), 7.79, 8.10, 8.12, 8.40, 8.59, 8.62, 8.86 (7 × vtr, 5 × 2H, 4H, 2H, $^3J$(HH) = 7 Hz, bipy-4,4′,5,5′), 8.47, 8.87, 8.93, 8.97, 9.03, 9.11, 9.32 (7 × d, 2H, 4H, 5 × 2H, $^3J$(HH) = 7 Hz, bipy-3,3′,6,6′). $^{13}$C NMR (100.6 MHz, DMSO-$d_8$): $\delta$ 6.0, 7.3 ($CH_3$), 68.8, 70.3, 74.6 ($C_5H_3$), 86.3, 87.2 ($C_5H_3$-*ipso*), 123.0, 123.1*, 123.5 (bipy-3,3′), 127.7, 128.3*, 129.0 (bipy-5,5′), 142.4, 142.5, 143.1, 143.5, 144.1*, 144.6, 144.8, 145.2, 145.5 (bipy-2,2′,4,4′,6,6′). Signals marked with an asterisk (*) possess a higher intensity due to the overlap of two or more unresolved resonances. Anal. Calcd for $C_{54}H_{50}B_4F_{24}FeN_8P_4 \cdot CH_3CN$ (1490.00 + 41.05): C, 43.93; H, 3.49; N, 8.23. Found: C, 44.03; H, 3.42; N, 8.38.

**X-ray Single-Crystal Structure Determination of [1A]PF$_6$.**[25] Suitable crystals were grown from $CH_3CN$/diethyl ether (1:1) at ambient temperature: $C_{21}H_{20}BF_6FeN_2P$, crystal size 0.86 × 0.61 × 0.20 mm; fw = 512.02; monoclinic space group $P2_1$ (No. 4), $a$ = 7.3075(5) Å, $b$ = 11.3931(7) Å, $c$ = 13.0388(11) Å, $\beta$ = 97.755(7)°, $V$ = 1075.6(1) Å$^3$, $Z$ = 2; $D_{calcd}$ = 1.581 g cm$^{-3}$; $F_{000}$ = 520; $\mu$ = 8.4 cm$^{-1}$. Crystal data together with details of the data collection and structure refinement are listed in Table 1. Preliminary examination and data collection were carried out on an imaging plate diffraction system (IPDS; Stoe&Cie) equipped with a rotating anode (Enraf-Nonius FR591; 50 kV; 80 mA; 4.0 kW) and graphite-monochromated Mo K$\alpha$ radiation ($\lambda$ = 0.710 73). The data collection was performed at 193 ± 1 K within the $\theta$-range of 2.4° < $\theta$ < 25.6° with an exposure time of 1 min per image (rotating scan modus from $\varphi$ = 0.0° to 199.0° with $\Delta\varphi$ = 1°). A total number of 8063 reflections were collected, from which a sum of 3971 independent reflections remained and were used for all calculations (12 systematically absent reflections rejected). Data were corrected for Lorentz and polarization effects.[48] Corrections for intensity decay and absorption effects are based on the program DECAY (SF = 3).[48] The unit cell parameters were obtained by least squares refinements of 1995 reflections with the program CELL.[48,49] The structure was solved by direct methods and refined by full-matrix least-squares calculations with anisotropic thermal parameters for all non-hydrogen atoms. All hydrogen atoms were calculated in ideal positions (riding model). Note: Disorder of the $PF_6^-$ octahedra leads to a superlattice problem and suggests a doubling of the unit cell's $c$ axis. However, refinement to a satisfactory level was achieved using the cell dimensions given above, and the molecular structure of the cationic moiety is well-defined. Full-matrix least-squares refinements were carried out by minimizing $\sum w(F_o^2 - F_c^2)^2$ with the SHELXL weighting scheme and stopped at shift/err < 0.001; wR2 = 0.1065 and R1 = 0.0448 for all data; *GOOF* = 1.056, 288 parameters, residual electron density +1.39 e Å$^{-3}$, −0.33 e Å$^{-3}$. Neutral atom scattering factors for all atoms and anomalous dispersion corrections for the non-hydrogen atoms were taken from the *International Tables for X-ray Crystallography*.[50] All calculations were performed on a DEC 3000 AXP workstation with the STRUX-V system,[51] including the programs PLATON-92,[52] PLUTON-92,[52] SIR-92,[53] and SHELXL-93.[54]

**X-ray Single-Crystal Structure Determination of [2A](PF$_6$)$_2$.**[25] Suitable crystals were grown from $CH_3CN$/diethyl ether (1:1) at ambient temperature: $C_{32}H_{30}B_2F_{12}FeN_4P_2$, crystal size 0.43 × 0.41 × 0.33 mm; fw = 838.02; monoclinic space group $P2_1/c$ (No. 14), $a$ = 9.1984(7) Å, $b$ = 14.8407(6) Å, $c$ = 12.1930(10) Å, $\beta$ = 100.851(4)°, $V$ = 1634.7(2) Å$^3$, $Z$ = 2; $D_{calcd}$ = 1.703 g cm$^{-3}$; $F_{000}$ = 848; $\mu$ = 55.6 cm$^{-1}$. Crystal data

---

(48) *IPDS Operating System*, Version 2.6; STOE&CIE. GmbH: Darmstadt, Germany, 1995.

(49) Schütt, W.; Herdtweck, E.; Hahn, F.; Kreissl, F. R. *J. Organomet. Chem.* **1993**, *443*, C33 and references cited therein.

(50) *International Tables for X-ray Crystallography*; Wilson, A. J. C., Ed.; Kluwer Academic Publishers: Dordrecht, 1992; Vol. C, Tables 4.2.4.2, 4.2.6.8, 6.1.1.4, pp 193−199, 219−222, 500−502.

(51) Artus, G.; Scherer, W.; Priermeier, T.; Herdtweck, E. *STRUX-V, A Program System to Handle X-ray Data*; TU München: München, Germany, 1994.

(52) Spek, A. L. *Acta Crystallogr.* **1990**, *A46*, C34.

(53) Altomare, A.; Cascarano, G.; Giacovazzo, C.; Guagliardi, A.; Burla, M. C.; Polidori, G.; Camalli, M. *SIR-92*; University of Bari, Italy.

(54) Sheldrick, G. M. *J. Appl. Crystallogr.*, *in press.*

together with details of the data collection and structure refinement are listed in Table 1. Preliminary examination and data collection were carried out on an automatic four circle diffractometer (CAD4, Enraf-Nonius) equipped with a sealed tube and graphite-monochromated Cu Kα ($\lambda = 1.541\,84$ Å) radiation. The data collection was performed at $163 \pm 1$ K within the $\theta$-range of $4.8° < \theta < 67.9°$ ($\theta/2\theta$ scan), maximal acquisition time 120 s for a single reflection. During data collection, a decay of 12.7% was observed. Data were corrected for $Lp$, linear decay and absorption effects ($T_{\mathrm{min/max}}$, 0.946/1.000). From the 6242 collected data, 249 (systematically absent) and 250 (negative intensity) were rejected. All 2913 ($R_{\mathrm{int}} = 0.0371$; $I > 0.0\,\sigma(I)$) unique data were used in the final refinement. The structure was solved by direct methods and refined by full-matrix least-squares calculations with anisotropic thermal parameters for all non-hydrogen atoms. All hydrogen atoms were located in the difference Fourier map and refined freely. The unit cell parameters were obtained by least-squares refinements of 25 high-angle reflections ($2\theta > 80°$). Full-matrix least-squares refinements were carried out by minimizing $\sum w(F_o^2 - F_c^2)^2$ with the SHELXL weighting scheme and stopped at shift/err < 0.001; wR2 = 0.0806 and R1 = 0.0325 for all data; *GOOF* = 1.067, 302 parameters, residual electron density +0.49 e Å$^{-3}$, −0.41 e Å$^{-3}$. Neutral atom scattering factors for all atoms and anomalous dispersion corrections for the non-hydrogen atoms were taken from the *International Tables for X-ray Crystallography*.[50] All calculations were performed on a DEC 3000 AXP workstation with the STRUX-V system,[51] including the programs PLATON-92,[52] PLUTON-92,[52] SIR-92,[53] and SHELXL-93.[54]

**X-ray Single Crystal Structure Determination of [4A]-Br₄.**[25] Suitable crystals were grown from ethanol (96%) at ambient temperature: $C_{54}H_{50}B_4Br_4FeN_8\cdot 7.75H_2O$, crystal size 0.43 × 0.26 × 0.26 mm; fw = 1369.37; monoclinic space group *C*2/*c* (No. 15), $a = 11.7038(7)$ Å, $b = 23.4915(10)$ Å, $c = 22.6688(17)$ Å, $\beta = 104.157(7)°$, $V = 6043.3(7)$ Å$^3$, $Z = 4$; $D_{\mathrm{calcd}} = 1.505$ g cm$^{-3}$; $F_{000} = 2774$; $\mu = 29.5$ cm$^{-1}$. Crystal data together with details of the data collection and structure refinement are listed in Table 1. Preliminary examination and data collection were carried out on an imaging plate diffraction system (IPDS; Stoe&Cie) equipped with a rotating anode (Enraf-Nonius FR591; 50 kV; 80 mA; 4.0 kW) and graphite-monochromated Mo Kα radiation ($\lambda = 0.710\,73$). The data collection was performed at $193 \pm 1$ K within the $\theta$-range of $2.0° < \theta < 25.6°$ with an exposure time of 3 min per image (rotating scan modus from $\varphi = 0.0°$ to $204.0°$ with $\Delta\varphi = 1°$). A total number of 23 364 reflections were collected, from which a sum of 5651 independent reflections remained and were used for all calculations (315 systematically absent reflections rejected). Data were corrected for Lorentz and polarization effects.[48] Corrections for intensity decay and absorption effects are based on the program DECAY (SF = 4).[48] The unit cell parameters were obtained by least-squares refinements of 4791 reflections with the program CELL.[48,49] The structure was solved by direct methods and refined by full-matrix least-squares calculations with anisotropic thermal parameters for all non-hydrogen atoms. All hydrogen atoms were calculated in ideal positions (riding model). Full-matrix least-squares refinements were carried out by minimizing $\sum w(F_o^2 - F_c^2)^2$ with the SHELXL weighting scheme and stopped at shift/err < 0.001; wR2 = 0.0840 and R1 = 0.0587 for all data; *GOOF* = 0.923, 360 parameters, residual electron density +0.71 e Å$^{-3}$, −0.46 e Å$^{-3}$. Neutral atom scattering factors for all atoms and anomalous dispersion corrections for the non-hydrogen atoms were taken from the *International Tables for X-ray Crystallography*.[50] All calculations were performed on a DEC 3000 AXP workstation with the STRUX-V system,[51] including the programs PLATON-92,[52] PLUTON-92,[52] SHELXS-86,[55] and SHELXL-93.[54]

**Electrochemical Measurments and ESR Spectroscopy.** Cyclic voltammetry and controlled-potential coulometry were performed in deaerated dimethylformamide (DMF) and $CH_2Cl_2$ solutions containing, respectively, [$NEt_4$][$PF_6$] and [$NBu_4$][$ClO_4$] (0.2 mol dm$^{-3}$) as the supporting electrolyte. All potential values are referred to the saturated calomel electrode (SCE).

The external magnetic field $H_0$ for ESR measurments was calibrated by using a DPPH powder sample ($g_{\mathrm{DPPH}} = 2.0036$). The apparatus for electrochemistry and coupled ESR measurments has been described in ref 56.

**Acknowledgment.** We are grateful to Prof. Dr. W. A. Herrmann (Technische Universität München) for his generous support. Financial funding by the “Deutsche Forschungsgemeinschaft” and the “Fonds der Chemischen Industrie” is acknowledged. P.Z. gratefully acknowledges the financial support by MURST of Italy (quota 40%).

**Supporting Information Available:** Tables of X-ray parameters, atomic coordinates and thermal parameters, and bond distances and angles (21 pages). Ordering information is given on any current masthead page.

OM970345Z

---

(55) Sheldrick, G. M. *SHELXS-86: Program for Crystal Structure Solutions*; Universität Göttingen: Göttingen, Germany, 1986.

(56) Bianchini, C.; Laschi, F.; Masi, D; Ottaviani, F. M.; Pastor, A; Peruzzini, M.; Zanello, P.; Zanobini, F. *J. Am. Chem. Soc.* **1993**, *115*, 2723.